

Beampattern Design for Transmit Architectures Based on Reconfigurable Intelligent Surfaces

Emanuele Grossi, *Senior Member, IEEE*, Luca Venturino, *Senior Member, IEEE*

Abstract—In this work, we tackle the problem of beampattern design for a transmit architecture wherein a large reconfigurable intelligent surface (RIS) redirects the radio frequency signals emitted by a few active antennas (sources). After introducing a convenient signal model and discussing the impact of the signal bandwidth, the source-RIS channel, and the system geometry on the involved derivations, we propose to optimize the waveform emitted by each source and the phase shifts introduced by the RIS to match a desired space-frequency distribution of the far-field radiation pattern, which may be relevant in both radar and communication applications. We provide a sub-optimum solution to the considered problem under a constraint on the total power radiated by the sources and, possibly, on the constant modulus of the involved waveforms. The reported example demonstrates that the beampattern of an RIS-based transmit architecture can be well shaped; in particular, for the same array size and the same desired radiation pattern, the resulting approximation error remains comparable to that obtained with a fully-digital MIMO array, especially when constant-modulus waveforms are required, and smaller than that obtained with a phased array.

Index Terms—Reconfigurable intelligent surface (RIS), intelligent reconfigurable surface (IRS), metasurfaces, beampattern design, radar, multiple-input multiple-output (MIMO) communications, integrated sensing and communication (ISAC).

I. INTRODUCTION

A classical problem in digital array processing is the synthesis of a desired transmit beampattern, i.e., a desired amplitude (or power) distribution in space and frequency of the far-field electromagnetic radiation, which is relevant in many wireless applications. For example, the synthesis of multiple beampatterns allows for beam scanning, target tracking, and track-while-scan operations in radar systems [1]. 5G and 6G communication systems operating at millimeter (mmWave), sub-THz, and THz bandwidths also employ directional beams to cope with the severe pathloss and, possibly, serve multiple users via a space-division multiple access [2]–[4]. An adequate shaping of the transmit beampattern can reduce the signal leakage towards eavesdroppers and mitigate the interference among different access points and/or radar systems operating in the same area [5]–[7]. Finally, in integrated sensing and communication (ISAC) systems, a dual-function transceiver may shape the desired beampattern to simultaneously monitor a given region and serve a communication user [8]–[10].

A large (massive) antenna array is often required or desired in the aforementioned applications. In this case, using fully

digital arrays, wherein each antenna is controlled by a dedicated radio frequency (RF) chain, may not be a viable option due to high cost and energy consumption [11]. Hybrid analog-digital arrays have been proposed in the past to reduce the number of required RF chains [12], [13]; here, the output of a few RF chains is connected via an analog network to either all antennas or a subset of them, thus resulting in fully- and partially-connected architectures, respectively. However, both these architectures are still hardly scalable with the number of antennas due to the power consumption of the involved analog network [14], [15].

Reconfigurable intelligent surfaces (RISs) have been recently proposed to address this problem and find energy-efficient techniques with low-cost hardware (e.g., metasurface-based transmitters in [16], RIS-aided antennas in [15], and transmitter-type RIS in [17]). An RIS is a planar array consisting of tunable elements that reflect the incident electromagnetic signal with a desired phase/amplitude adjustment without using RF chains or introducing a processing delay. RISs can be either passive [18]–[22] or active [23]–[25] and can be controlled and reconfigured almost in real time [26]. They can be either reflecting (where the signal is reflected from the surface) or transmitting (where the signal is transmitted in the forward direction),¹ but, more recently, simultaneously reflecting and transmitting RISs have been also considered [30]. RISs can be deployed either far away from or in close proximity to the transmitting source. In the former case, the RIS is part of the wireless channel that can be dynamically controlled so that a smart radio environment can be realized [16], [31]–[35]. In the latter case, instead, the RIS is embedded into the transmit architecture; namely, the whole system acts as a feed antenna, and the channel between the source and the RIS is fixed and can be properly designed during manufacturing [36]–[38].

In this work, we tackle the problem of beampattern design for the RIS-based transmit architecture introduced in [15], [39], where a few active antennas called sources (possibly one, as in [39]), each equipped with a dedicated RF chain, illuminate a (passive) RIS, composed of a large number of low-cost and energy-efficient elements, that reflect/retransmit a phase-shifted version of the superposition of the signals emitted by the sources. These types of architectures have many advantages [15]. Indeed, the beam-steering capability

¹The main difference between reflective and transmitting RIS is that the latter uses a pair of patches (one in each half-plane) for receiving and transmitting, whereas the former reuses the same patch for receiving and reflecting [15], [27]; nevertheless, both types can accurately be described by the same equivalent lumped circuit model [28], [29]. In general, reflective RISs are less complex (thanks to the easier placement of the control system for the phase shifters on the back side of the surface) and have a larger gain (due to the metal ground plane that reflects the entire incident wave).

The authors are with the Department of Electrical and Information Engineering (DIEI), University of Cassino and Southern Lazio, 03043 Cassino, Italy, and with Consorzio Nazionale Interuniversitario per le Telecomunicazioni (CNIT), 43124 Parma, Italy (e.grossi@unicas.it; l.venturino@unicas.it).

is directly controlled by the RIS, so the number of active antennas does not have to scale with the number of passive elements in the RIS. Furthermore, contrary to what happens in hybrid analog-digital arrays, where the analog network which feeds the transmit antennas causes a severe power loss that prevents its implementation in massive MIMO and high-frequency systems [36], in this RIS-based transmit architecture the source-RIS channel is wireless and is referred to as *space feeding mechanism*, that is inherently more energy-efficient [20], [36].

The design of the transmit beampattern of an antenna array is a classical problem that has already been studied in the context of MIMO radars, either for narrowband [40]–[44] or broadband [45]–[48] array configurations, and in biomedical imaging [49]: in these cases, the probing waveforms are designed so that the realized beampattern matches, in a least-square sense, the desired one. This problem has also been addressed in DFRC systems [8], [50]–[53], but, in the latter case, only the radar beampattern has been designed. To the best of the authors’ knowledge, the beampattern design problem for the considered RIS-based transmit architecture has been considered only in [54] for a narrowband system with a single source and with no waveform design. In this context, leveraging the preliminary results reported in [55], we make the following contributions.²

- We develop a detailed model for the far-field signal of the RIS-based transmit architecture, eliciting the effects of the waveforms emitted by the active sources, the RIS adjustable phases, and the source-RIS channels.
- We discuss the cases when this architecture is narrowband or broadband, eliciting the impact of the RIS size, location of the sources, and signal bandwidth.
- We present and formulate the transmit beampattern design problem for this architecture, where the waveforms emitted by the sources and the phase shifts introduced by the RIS are jointly optimized; different constraints on the source signals are considered, including the constant-modulus constraint, which is a key requirement for efficiency when saturated power amplifiers are used.
- We show that beampattern design problem, although different from those considered in other related works, can be tackled with consolidated methodologies, and we present a sub-optimum solution.
- Finally, we provide a few examples showing that this architecture can be competitive compared to fully digital MIMO systems in terms of synthesized beampattern, especially if the constant-modulus constraint is enforced.

Use cases for this RIS-based transmit architecture are radars, where the exploitation of RISs has already been advocated in [56]–[59] for improving the radar performance or reducing the costs, in communication and DFRC systems [60]–[62], where the selection of one among different beampatterns allows for a spatial/beam index modulation, and in (massive)

²The present contribution differs from [55] in several respects: the system description is enriched with more details and with a critical discussion on the narrowband and broadband operating conditions; the additional constant-modulus constraint is considered; the analytical derivation of all proposed solutions is given; and, finally, a richer numerical analysis is provided.

MIMO communication systems [15], when broadcasting control signals are to be sent. Finally, the results found here apply both to the case where the sources are close to the RIS (thus forming a unique physical device) and to the case where the sources are far away from the RIS: in this latter scenario, the sources can also be represented by different systems (e.g., base stations or radars) that cooperate together and devote some of their physical resources (i.e., a narrow beam pointing towards the RIS in some specific frequency intervals) to sense an area that is not in the field-of-view of their transmitters and/or communicate with terminals located in such an area.

The remainder of the paper is organized as follows. In Sec. II, the considered transmit RIS-based architecture is described, and the beampattern is derived. In Sec. III, the beampattern matching problem is presented, and a suboptimal solution is found. In Sec. IV, a numerical example is presented to demonstrate the advantages of the proposed approach compared to other standard benchmarks. Finally, concluding remarks and future research lines are highlighted in Sec. V.

Notation: In the following, \mathbb{R} and \mathbb{C} denote the set of real and complex numbers, respectively, while i is the imaginary unit; $\Re(a)$ is the real part of $a \in \mathbb{C}$; vectors and matrices are denoted by lowercase and uppercase boldface letters, respectively; $\mathbf{A} \succ 0$ means that the matrix \mathbf{A} is Hermitian positive semidefinite; $(\cdot)^*$, $(\cdot)^T$, and $(\cdot)^H$ denote conjugate, transpose, and conjugate transpose, respectively; \mathbf{I}_n is the $n \times n$ identity matrix; $\text{diag}(\mathbf{a})$ is the diagonal matrix with entries \mathbf{a} on the main diagonal; $\|\cdot\|$ denotes the Euclidean norm; $\mathbb{E}[\cdot]$ denotes statistical expectation; $\mathcal{O}(\cdot)$ is the big-O notation, to asymptotically bound a function from above; $\mathcal{P}_T(\mathbf{a})$ is the projection of $\mathbf{a} \in \mathbb{C}^n$ on the n -dimensional unit-modulus torus, i.e., $\mathcal{P}_T(\mathbf{a}) = \mathbf{b} \in \mathbb{C}^n$, with $b_i = a_i/|a_i|$, if $a_i \neq 0$, and any unit-modulus complex scalar, otherwise; finally, $\mathcal{P}_{B,r}(\mathbf{a})$ is the projection of $\mathbf{a} \in \mathbb{C}^n$ on the n -dimensional ball with radius r , i.e., $\mathcal{P}_{B,r}(\mathbf{a}) = (r/\|\mathbf{a}\|)\mathbf{a}$, if $\|\mathbf{a}\| \geq r$, and $\mathcal{P}_{B,r}(\mathbf{a}) = \mathbf{a}$, otherwise.

II. SYSTEM DESCRIPTION

Consider a transmit architecture composed of an illuminator with J elements (also called sources) and a passive RIS with M elements, as shown in Fig. 1. The carrier frequency is f_c , and the lowpass signal emitted by the j -th source of the illuminator is denoted $s_j(t)$: it is a waveform with support included in the interval $[0, T]$ and Fourier transform approximately equal to zero outside the interval $[-W/2, W/2]$. The i -th element of the RIS is located at position \mathbf{p}_i and introduces a (controllable) phase shift that is modeled by³ the unit-modulus complex value x_i . The global reference system is located at the center of gravity of the RIS, so that $\sum_{i=1}^M \mathbf{p}_i = [0\ 0\ 0]^T$. The frequency response of the channel linking the j -th source, the i -th element of the RIS, and the point (r, θ, φ) in the far-field region is⁴

$$H_{ij}(f; r, \theta, \varphi) = \frac{e^{-2\pi i f(r/c + \tau_i(\theta, \varphi))}}{\sqrt{4\pi r^2}} \Gamma_i(\theta, \varphi) x_i G_{ij}(f), \quad (1)$$

³We are assuming here that W is sufficiently small that the frequency response of the RIS can be considered constant in $[-W/2, W/2]$.

⁴We are assuming here that the possible coupling effects among the element of the RIS and the sources can be neglected.

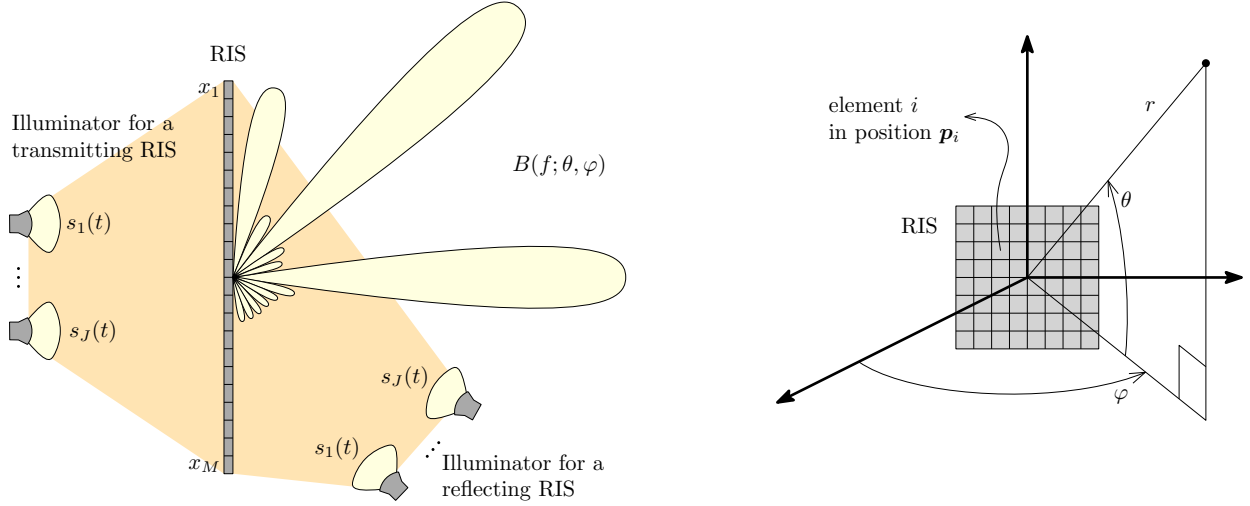


Figure 1. Beampattern at frequency f and spatial angle (θ, φ) of a transmit architecture composed of illuminator with J elements and an RIS with M elements. The illuminator can be located behind the surface (for a transmitting RIS) or in front of it (for a reflecting RIS).

where $G_{ij}(f)$ is the frequency response of the channel between source j and element i of the RIS, x_i models the frequency response of the RIS, and the remaining terms represent the frequency response of the channel between element i of the RIS and the observation point; in particular, $\Gamma_i(\theta, \varphi)$ is the amplitude beampattern of element i of the RIS in the direction (θ, φ) , $\sqrt{4\pi r^2}$ is the term due to the free-space attenuation from the RIS to the observation point, and $r/c + \tau_i(\theta, \varphi)$ is the corresponding propagation delay, with c denoting the speed of light and [63, Eq. (2.16)]

$$\tau_i(\theta, \varphi) = -\frac{1}{c}(p_{i,1} \cos \theta \cos \varphi + p_{i,2} \cos \theta \sin \varphi + p_{i,3} \sin \theta). \quad (2)$$

With this notation, the Fourier transform of the complex envelope of the signal observed at (r, θ, φ) is

$$\begin{aligned} Y(f; r, \theta, \varphi) &= \sum_{i=1}^M \sum_{j=1}^J H_{ij}(f + f_c; r, \theta, \varphi) S_j(f) \\ &= \frac{e^{-2\pi i(f+f_c)r/c}}{\sqrt{4\pi r^2}} \sum_{i=1}^M e^{-2\pi i(f+f_c)\tau_i(\theta, \varphi)} \\ &\quad \times \Gamma_i(\theta, \varphi) x_i \sum_{j=1}^J G_{ij}(f + f_c) S_j(f), \quad (3) \end{aligned}$$

where $S_j(f)$ is the Fourier transform of $s_j(t)$. Letting

$$\mathbf{x} = [x_1 \cdots x_M]^T \in \mathbb{C}^M, \quad (4)$$

$$\boldsymbol{\sigma}(f) = [S_1(f) \cdots S_J(f)]^T \in \mathbb{C}^J, \quad (5)$$

and denoting by $\boldsymbol{\Omega}(f; \theta, \varphi)$ the $M \times J$ complex matrix with entry (i, j) $\Omega_{ij}(f; \theta, \varphi) = G_{ij}(f + f_c)\Gamma_i(\theta, \varphi)$, we can rewrite (3) in the following compact form

$$\begin{aligned} Y(f; r, \theta, \varphi) &= \frac{1}{\sqrt{4\pi r^2}} e^{-2\pi i(f+f_c)r/c} \\ &\quad \times \mathbf{v}^H(f; \theta, \varphi) \text{diag}(\mathbf{x}) \boldsymbol{\Omega}(f; \theta, \varphi) \boldsymbol{\sigma}(f), \quad (6) \end{aligned}$$

where

$$\mathbf{v}(f; \theta, \varphi) = [e^{2\pi i(f+f_c)\tau_1(\theta, \varphi)} \cdots e^{2\pi i(f+f_c)\tau_M(\theta, \varphi)}]^T \in \mathbb{C}^M \quad (7)$$

is the array manifold vector in the direction (θ, φ) at frequency f [63, Eq. (6.669)]. Therefore, the amplitude beampattern at frequency f and spatial angle (θ, φ) is⁵

$$\begin{aligned} B(f; \theta, \varphi) &= \sqrt{\frac{4\pi r^2}{T}} |Y(f; r, \theta, \varphi)| \\ &= \frac{1}{\sqrt{T}} |\mathbf{v}^H(f; \theta, \varphi) \text{diag}(\mathbf{x}) \boldsymbol{\Omega}(f; \theta, \varphi) \boldsymbol{\sigma}(f)|. \quad (8) \end{aligned}$$

Since the signals emitted by the sources are bandlimited, i.e., $|S_j(f)| \approx 0$ for all $f \notin [-W/2, W/2]$, we have that

$$S_j(f) = \int_0^T s_j(t) e^{-2\pi i f t} dt \approx \frac{1}{W} \sum_{n=1}^N s_j(n/W) e^{-2\pi i n f / W}, \quad (9)$$

where $N = \lfloor WT \rfloor$. Therefore, upon defining

$$\mathbf{s}_n = [s_1(n/W) \cdots s_J(n/W)]^T \in \mathbb{C}^J, \quad (10)$$

$$\mathbf{s} = [\mathbf{s}_1^T \cdots \mathbf{s}_N^T]^T \in \mathbb{C}^{JN}, \quad (11)$$

we can finally approximate (8) as

$$\begin{aligned} B(f; \theta, \varphi) &\approx \frac{1}{W\sqrt{T}} \left| \mathbf{v}^H(f; \theta, \varphi) \text{diag}(\mathbf{x}) \boldsymbol{\Omega}(f; \theta, \varphi) \right. \\ &\quad \left. \times \sum_{n=1}^N \mathbf{s}_n e^{-2\pi i n f / W} \right| \\ &= \frac{1}{W\sqrt{T}} \left| \mathbf{v}^H(f; \theta, \varphi) \text{diag}(\mathbf{x}) \boldsymbol{\Omega}(f; \theta, \varphi) (\mathbf{e}^T(f) \otimes \mathbf{I}_J) \mathbf{s} \right| \\ &= |\mathbf{v}^H(f; \theta, \varphi) \text{diag}(\mathbf{x}) \mathbf{Q}(f; \theta, \varphi) \mathbf{s}|, \quad (12) \end{aligned}$$

⁵The power spectral density of a (deterministic) signal is obtained by dividing the squared modulus of its Fourier transform (i.e., the energy spectral density) by the signal duration (i.e., T). Since we consider the amplitude beampattern, we divide the modulus of the Fourier transform by \sqrt{T} .

where

$$\mathbf{e}(f) = [e^{-2\pi i f/W} \dots e^{-2\pi i N f/W}]^T \in \mathbb{C}^N, \quad (13)$$

$$\mathbf{Q}(f; \theta, \varphi) = \frac{1}{W\sqrt{T}} \boldsymbol{\Omega}(f; \theta, \varphi) (\mathbf{e}^T(f) \otimes \mathbf{I}_J) \in \mathbb{C}^{M \times JN}. \quad (14)$$

Observe that (8) and (12) represent an extension to the considered RIS-based architecture of the amplitude beampattern for MIMO systems analyzed in [46].

A. Narrowband/broadband architectures

In general, the channel between source j and element i of the RIS can be modeled as a tap-delay line, i.e.,

$$G_{ij}(f) \approx \sum_{\ell=1}^{L_{ij}} g_{ij\ell} e^{-2\pi i f t_{ij\ell}}, \quad (15)$$

where L_{ij} is the number of taps, $g_{ij\ell}$ and $t_{ij\ell}$ are the attenuation and delay of the ℓ -th tap, respectively, and $\max_{\ell} t_{ij\ell} - \min_{\ell} t_{ij\ell}$ is the delay spread. Upon defining

$$\delta = \frac{1}{2} \left(\max_{i,j,\ell} t_{ij\ell} + \min_{i,j,\ell} t_{ij\ell} \right), \quad (16a)$$

$$\delta_{ij\ell} = t_{ij\ell} - \delta, \quad \forall i, j, \ell, \quad (16b)$$

the complex envelope in (3) can be rewritten as

$$\begin{aligned} Y(f; r, \theta, \varphi) &\approx \frac{e^{-2\pi i(f+f_c)(r/c+\delta)}}{\sqrt{4\pi r^2}} \sum_{i=1}^M e^{-2\pi i f_c \tau_i(\theta, \varphi)} \\ &\times \Gamma_i(\theta, \varphi) x_i \sum_{j=1}^J \sum_{\ell=1}^{L_{ij}} g_{ij\ell} e^{-2\pi i f_c \delta_{ij\ell}} \\ &\times S_j(f) e^{-2\pi i f(\tau_i(\theta, \varphi) + \delta_{ij\ell})}. \end{aligned} \quad (17)$$

If the delay offset $|\tau_i(\theta, \varphi) + \delta_{ij\ell}|$ is sufficiently small to have

$$e^{-2\pi i f(\tau_i(\theta, \varphi) + \delta_{ij\ell})} \approx 1, \quad \forall f \in [f_c - W/2, f_c + W/2], \quad (18)$$

then (17) can further be approximated as

$$\begin{aligned} Y(f; r, \theta, \varphi) &\approx \frac{e^{-2\pi i(f+f_c)(r/c+\delta)}}{\sqrt{4\pi r^2}} \sum_{i=1}^M e^{-2\pi i f_c \tau_i(\theta, \varphi)} \\ &\times \Gamma_i(\theta, \varphi) x_i \sum_{j=1}^J \left(\sum_{\ell=1}^{L_{ij}} g_{ij\ell} e^{-2\pi i f_c \delta_{ij\ell}} \right) S_j(f). \end{aligned} \quad (19)$$

Notice that, in the time-domain, (19) becomes

$$\begin{aligned} y(t; r, \theta, \varphi) &\approx \frac{e^{-2\pi i f_c(r/c+\delta)}}{\sqrt{4\pi r^2}} \sum_{i=1}^M e^{-2\pi i f_c \tau_i(\theta, \varphi)} \Gamma_i(\theta, \varphi) x_i \\ &\times \sum_{j=1}^J \left(\sum_{\ell=1}^{L_{ij}} g_{ij\ell} e^{-2\pi i f_c \delta_{ij\ell}} \right) s_j(t - r/c - \delta), \end{aligned} \quad (20)$$

which shows that the signals $\{s_j(t)\}_{j=1}^J$ are now all delayed by the same quantity $r/c + \delta$ at the observation point and that the delay differences $\tau_i(\theta, \varphi) + \delta_{ij\ell}$ simply reduce to phase shifts, for all $\theta, \varphi, i, j, \ell$.

The approximations in (18), (19), and (20) are valid if

$$W \max_{\theta, \varphi} \left\{ \max_i \left(\tau_i(\theta, \varphi) + \max_{j,\ell} \delta_{ij\ell} \right) - \min_i \left(\tau_i(\theta, \varphi) + \min_{j,\ell} \delta_{ij\ell} \right) \right\} \ll 1. \quad (21)$$

If (21) is satisfied, we say that the RIS-based architecture is *narrowband*; otherwise, we say that it is *broadband*. Notice that (21) is a generalization of the well-known narrowband array condition [63, Eq. (2.47)] to the considered architecture, as it also accounts for the propagation delay offsets $\{\delta_{ij\ell}\}_{ij\ell}$ along the source-RIS channels.

Example 1. Consider a square planar RIS, with element field-of-view of 120° , illuminated by four point-like sources emitting signals with bandwidth $W = 75$ MHz; the sources are located at the same distance from the RIS in correspondence of its four corners, and $G_{ij}(f)$ contains only the line-of-sight path, for all i, j . Then, the left-hand side of (21) is equal to 0.49, if the sources-RIS distances and the side length of the RIS are 1 m, while it is equal to 0.098, if they are reduced to 20 cm: in the former case, the system is broadband, while in the latter it is narrowband.

Remark 1. When the sources are closely spaced, a good rule of thumb for the narrowband condition can be found by upper bounding the left-hand side of (21). To this end, let Δ_{RIS} and Δ_{sources} be the diameters of the smallest balls circumscribing the RIS and the sources, respectively. Then⁶

$$\begin{aligned} &\max_{\theta, \varphi} \left\{ \max_i \left(\tau_i(\theta, \varphi) + \max_{j,\ell} \delta_{ij\ell} \right) - \min_i \left(\tau_i(\theta, \varphi) + \min_{j,\ell} \delta_{ij\ell} \right) \right\} \\ &\leq \max_{\theta, \varphi} \left(\max_i \tau_i(\theta, \varphi) - \min_i \tau_i(\theta, \varphi) \right) \\ &\quad + \max_{i,j,\ell} \delta_{ij\ell} - \min_{i,j,\ell} \delta_{ij\ell} \\ &\leq \frac{\Delta_{\text{RIS}}}{c} + \frac{\Delta_{\text{RIS}} + \Delta_{\text{sources}}}{c}, \end{aligned} \quad (22)$$

and a sufficient condition for the narrowband condition in (21) to hold is⁷

$$2\Delta_{\text{RIS}} + \Delta_{\text{sources}} \ll c/W. \quad (23)$$

This can best be appreciated if compared with the equivalent sufficient condition for MIMO systems, namely, $\Delta_{\text{MIMO}} \ll c/W$, where Δ_{MIMO} is the diameters of the smallest balls circumscribing the fully digital array: indeed, (23) accounts now for the presence of two arrays (the RIS and the sources) and for the fact that the wave travels twice over the RIS (source-RIS and RIS-observation point).

By comparing (19) with (3), we see that, in the narrowband case, the amplitude beampattern retains the same expression as in (8) and (12), but the array manifold vector and the

⁶Observe that the first inequality in (22) comes from the fact that the maximum (minimum) of a sum is always smaller (greater) than the sum of the maxima (minima), while the second inequality is an upper bound obtained when the wave is parallel to the RIS, and sources and RIS lie in the same plane, whereby $\max_{\theta, \varphi} (\max_i \tau_i(\theta, \varphi) - \min_i \tau_i(\theta, \varphi)) = \Delta_{\text{RIS}}/c$ and $\max_{i,j,\ell} \delta_{ij\ell} - \min_{i,j,\ell} \delta_{ij\ell} = (\Delta_{\text{RIS}} + \Delta_{\text{sources}})/c$.

⁷Notice that c/W is the approximate range resolution of a waveform with bandwidth W .

source-RIS channels are now frequency independent; namely, $\mathbf{v}(f; \theta, \varphi)$ becomes

$$\mathbf{v}(\theta, \varphi) = [e^{2\pi i f_c \tau_1(\theta, \varphi)} \dots e^{2\pi i f_c \tau_M(\theta, \varphi)}]^\top, \quad (24)$$

and $\mathbf{\Omega}(f; \theta, \varphi)$ becomes $\mathbf{\Omega}(\theta, \varphi)$, with entry (i, j) given by

$$\Omega_{ij}(\theta, \varphi) = \Gamma_i(\theta, \varphi) \sum_{\ell=1}^{L_{ij}} g_{ij\ell} e^{-2\pi i f_c \delta_{ij\ell}}. \quad (25)$$

In this case, the dependency of the power distribution from the frequency is determined solely by the source signals and is often removed by integration, i.e.,

$$\begin{aligned} \bar{B}^2(\theta, \varphi) &= \int_{-W/2}^{W/2} B^2(f; \theta, \varphi) df \\ &= \mathbf{v}^H(\theta, \varphi) \text{diag}(\mathbf{x}) \mathbf{\Omega}(\theta, \varphi) \left(\frac{1}{T} \int_{-W/2}^{W/2} \boldsymbol{\sigma}(f) \boldsymbol{\sigma}^H(f) df \right) \\ &\quad \times \mathbf{\Omega}^H(\theta, \varphi) \text{diag}(\mathbf{x}^*) \mathbf{v}(\theta, \varphi). \end{aligned} \quad (26)$$

Since

$$\begin{aligned} \left(\frac{1}{T} \int_{-W/2}^{W/2} \boldsymbol{\sigma}(f) \boldsymbol{\sigma}^H(f) df \right)_{hk} &= \frac{1}{T} \int_{-W/2}^{W/2} S_h(f) S_k^*(f) df \\ &= \frac{1}{T} \int_0^T s_h(t) s_k^*(t) dt \\ &\approx \frac{1}{WT} \sum_{n=1}^N s_h \left(\frac{n}{W} \right) s_k^* \left(\frac{n}{W} \right) \\ &\approx \left(\frac{1}{N} \sum_{n=1}^N \mathbf{s}_n \mathbf{s}_n^H \right)_{hk}, \quad \forall h, k, \end{aligned} \quad (27)$$

where the last approximation follows from the fact that $N = \lfloor WT \rfloor$, we have that

$$\begin{aligned} \bar{B}^2(\theta, \varphi) &= \mathbf{v}^H(\theta, \varphi) \text{diag}(\mathbf{x}) \mathbf{\Omega}(\theta, \varphi) \left(\frac{1}{N} \sum_{n=1}^N \mathbf{s}_n \mathbf{s}_n^H \right) \\ &\quad \times \mathbf{\Omega}^H(\theta, \varphi) \text{diag}(\mathbf{x}^*) \mathbf{v}(\theta, \varphi). \end{aligned} \quad (28)$$

Observe that (28) represents an extension to the considered RIS-based architecture of the power beampattern over the space domain for MIMO systems analyzed in [40].

B. Asynchronous sources

When source signal j has support in $[\Delta_j, \Delta_j + T]$, where $\Delta_j \geq 0$ accounts for some initial transmission offset, we have

$$\begin{aligned} S_j(f) &= \int_{\Delta_j}^{\Delta_j+T} s_j(t) e^{-2\pi i f t} dt \\ &= e^{-2\pi i f \Delta_j} \int_0^T s_j(\Delta_j + t) e^{-2\pi i f t} dt \\ &\approx \frac{e^{-2\pi i f \Delta_j}}{W} \sum_{n=1}^N s_j(\Delta_j + n/W) e^{-2\pi n f / W}, \end{aligned} \quad (29)$$

for $j = 1, \dots, J$. In this case, our model still remains valid upon absorbing the phase term $e^{-2\pi i f \Delta_j}$ into the channel $G_{ij}(f)$ and defining \mathbf{s}_n in (11) as

$$\mathbf{s}_n = [s_1(\Delta_1 + n/W) \dots s_J(\Delta_J + n/W)]^\top \in \mathbb{C}^J, \quad (30)$$

for $n = 1, \dots, N$. For example, introducing some delay offsets may be desirable when the sources are located at different distances from the center of gravity of the RIS; in particular, closer sources may be delayed to ensure that all signals simultaneously reach the center of gravity of the RIS.

III. SYSTEM OPTIMIZATION

The objective here is to design the signal emitted by the illuminator \mathbf{s} and the RIS phases \mathbf{x} in such a way that the amplitude beampattern $B(f; \theta, \varphi)$ matches in a least squares (LS) sense the desired amplitude beampattern, say $D(f; \theta, \varphi)$. The LS amplitude beampattern matching is a well-accepted design criterion that has been extensively used in recent years (see, e.g., [46]). All following derivations rely on the general expression of the amplitude beampattern given in (12), so that they apply to both broadband and narrowband RIS-based architectures.

To proceed, define the relative square error (RSE) between the desired beam pattern and the actual beam pattern over the angular and frequency space as

$$\begin{aligned} \text{RSE}(\mathbf{s}, \mathbf{x}) &= \frac{1}{4\pi} \int_{-W/2}^{W/2} \int_{-\pi/2}^{\pi/2} \int_{-\pi/2}^{\pi/2} \tilde{w}(f; \theta, \varphi) \\ &\quad \times (D(f; \theta, \varphi) - B(f; \theta, \varphi))^2 \cos \theta d\theta d\varphi df \\ &\quad \times \left(\frac{1}{4\pi} \int_{-W/2}^{W/2} \int_{-\pi/2}^{\pi/2} \int_{-\pi/2}^{\pi/2} \tilde{w}(f; \theta, \varphi) \right. \\ &\quad \left. \times D^2(f; \theta, \varphi) \cos \theta d\theta d\varphi df \right)^{-1}, \end{aligned} \quad (31)$$

where $\tilde{w}(f; \theta, \varphi)$ is a weighting function that allows for the emphasis of different regions; observe that, if $\tilde{w}(f; \theta, \varphi) = 1$, the denominator is simply the power radiated with the desired beampattern. If we discretize the angular region $[-\pi/2, \pi/2]^2$ using a rectangular grid with L points uniformly-spaced along each dimension, namely $\{(\theta_\ell, \varphi_\ell)\}_{\ell=1}^L$, and the frequency region $[-W/2, W/2]$ using K uniformly-spaced points, namely $\{f_k\}_{k=1}^K$, the RSE can be approximated as

$$\begin{aligned} \text{RSE}(\mathbf{s}, \mathbf{x}) &\approx \sum_{k=1}^K \sum_{\ell=1}^L w(f_k; \theta_\ell, \varphi_\ell) \\ &\quad \times (D(f_k; \theta_\ell, \varphi_\ell) - B(f_k; \theta_\ell, \varphi_\ell))^2, \end{aligned} \quad (32)$$

where

$$\begin{aligned} w(f; \theta, \varphi) &= \frac{W\pi^2}{KL} \tilde{w}(f; \theta, \varphi) \cos \theta \\ &\quad \times \left(\int_{-W/2}^{W/2} \int_{-\pi/2}^{\pi/2} \int_{-\pi/2}^{\pi/2} \tilde{w}(f'; \theta', \varphi') \right. \\ &\quad \left. \times d^2(f'; \theta', \varphi') \cos \theta d\theta' d\varphi' df' \right)^{-1}. \end{aligned} \quad (33)$$

Hence, the beampattern matching problem tackled here is

$$\begin{aligned} &\min_{\mathbf{s} \in \mathbb{C}^{JN}, \mathbf{x} \in \mathbb{C}^M} \text{RSE}(\mathbf{s}, \mathbf{x}), \\ &\text{s.t. } \frac{1}{N} \|\mathbf{s}\|^2 \leq P, \\ &\quad |x_i| = 1, \quad i = 1, \dots, M, \end{aligned} \quad (34)$$

where P is the total power available at the illuminator.⁸ Notice that this problem differs from that usually considered in MIMO radars since the beampattern is not only a function of the steering vector (from the array to the observation point) but also of the source-RIS channels, and the degrees of freedom are not only the waveforms radiated by the active sources but also include the RIS adjustable phases. For notational convenience, we let

$$w_{k\ell} = w(f_k; \theta_\ell, \varphi_\ell), \quad D_{k\ell} = D(f_k; \theta_\ell, \varphi_\ell), \quad (35a)$$

$$\mathbf{v}_{k\ell} = \mathbf{v}(f_k; \theta_\ell, \varphi_\ell), \quad \mathbf{Q}_{k\ell} = \mathbf{Q}(f_k; \theta_\ell, \varphi_\ell), \quad (35b)$$

for $k = 1, \dots, K$ and $\ell = 1, \dots, L$, so that Problem (34) can be equivalently rewritten as

$$\begin{aligned} \min_{\mathbf{s} \in \mathbb{C}^{JN}, \mathbf{x} \in \mathbb{C}^M} & \sum_{k=1}^K \sum_{\ell=1}^L w_{k\ell} (D_{k\ell} - |\mathbf{v}_{k\ell}^H \text{diag}(\mathbf{x}) \mathbf{Q}_{k\ell} \mathbf{s}|)^2, \\ \text{s.t. } & \|\mathbf{s}\|^2 \leq NP, \\ & |x_i| = 1, \quad i = 1, \dots, M. \end{aligned} \quad (36)$$

Problem (36) is intractable due to the non-differentiability of the objective function (caused by the absolute value), and a common approach [46] is to exploit the fact that, for any $a > 0$ and $b \in \mathbb{C}$,

$$\min_{\psi \in \mathbb{R}} |ae^{i\psi} - b|^2 = (a - |b|)^2, \quad \text{for } \psi = \arg b. \quad (37)$$

As a consequence, upon introducing the auxiliary variables $\{\psi_{k\ell}\}$, Problem (36) can be equivalently rewritten as

$$\begin{aligned} \min_{\substack{\mathbf{s} \in \mathbb{C}^{JN}, \mathbf{x} \in \mathbb{C}^M, \\ \{\psi_{k\ell}\} \in \mathbb{R}^{KL}}} & \sum_{k=1}^K \sum_{\ell=1}^L w_{k\ell} |D_{k\ell} e^{i\psi_{k\ell}} - \mathbf{v}_{k\ell}^H \text{diag}(\mathbf{x}) \mathbf{Q}_{k\ell} \mathbf{s}|^2, \\ \text{s.t. } & \|\mathbf{s}\|^2 \leq NP, \\ & |x_i| = 1, \quad i = 1, \dots, M. \end{aligned} \quad (38)$$

This problem is still very complex due to the non-convexity of both the objective function and the constraint set, and an optimal solution is not available, whereby we resort to sub-optimal procedures to solve it. In particular, we tackle it by resorting to the block-coordinate descent method [64], also known as non-linear Gauss-Seidel method or as alternating minimization: starting from a feasible point, the objective function is minimized with respect to each of the ‘‘block coordinate’’ variables, taken in cyclic order while keeping the other ones fixed at their previous values.

Here, the *natural* block-coordinate variables are the auxiliary variables $\{\psi_{k\ell}\}_{k,\ell}$, the illuminator signals \mathbf{s} , and the RIS phases \mathbf{x} . The auxiliary variables can be disjointly minimized, and, from (37), the solution is⁹

$$\psi_{k\ell} = \arg(\mathbf{v}_{k\ell}^H \text{diag}(\mathbf{x}) \mathbf{Q}_{k\ell} \mathbf{s}), \quad (39)$$

⁸We have chosen here a *global* power constraint, but individual power constraints (more suited when the sources are widely spaced from each other and from the RIS) can similarly be handled. In this case, $N^{-1} \|\mathbf{s}\|^2 \leq P$ would be replaced by $N^{-1} \sum_{n=1}^N |s_{j+(n-1)J}|^2 \leq P_j$, $j = 1, \dots, J$, where P_j is the available power at source j .

⁹Notice that the computational complexity for updating $\{\psi_{k\ell}\}_{k,\ell}$ is $\mathcal{O}(KLMJN)$.

Algorithm 1 Block-coordinate descent for Problem (38)

```

choose  $\mathbf{s} \in \mathbb{C}^{JN} : \|\mathbf{s}\|^2 \leq NP$ 
choose  $\mathbf{x} \in \mathbb{C}^M : |x_i| = 1 \ \forall i$ 
 $\psi_{k\ell} = \arg(\mathbf{v}_{k\ell}^H \text{diag}(\mathbf{x}) \mathbf{Q}_{k\ell} \mathbf{s}), \ \forall k, \ell$ 
repeat
  update  $\mathbf{s}$  as in Sec. III-A
  update  $\mathbf{x}$  as in Sec. III-B
   $\psi_{k\ell} = \arg(\mathbf{v}_{k\ell}^H \text{diag}(\mathbf{x}) \mathbf{Q}_{k\ell} \mathbf{s}), \ \forall k, \ell$ 
until convergence
return  $\mathbf{s}$  and  $\mathbf{x}$ 

```

for $k = 1, \dots, K$ and $\ell = 1, \dots, L$. The solution to the remaining two sub-problems (minimization over \mathbf{s} and over \mathbf{x}) is provided in Secs. III-A and III-B, and the complete routine is reported in Alg. 1. Notice that, with proper initialization of the algorithm used for the \mathbf{x} -update step (see Sec. III-B), the objective function is non-increasing in successive minimizations, so that Alg. 1 converges. However, since Problem (38) is not convex, and the feasible set cannot be expressed as the Cartesian product of closed convex sets, there is no guarantee that a global minimum is reached. It should also be noticed that alternative choices of the block-coordinate variables are possible, and, in Appendix A, another example is provided. Finally, in Sec. III-C, we tackle the case where a constant-modulus constraint is imposed on the illuminator signals.

A. Minimization over the illuminator signals

Upon defining

$$\mathbf{A} = \sum_{k=1}^K \sum_{\ell=1}^L w_{k\ell} \mathbf{Q}_{k\ell}^H \text{diag}(\mathbf{x}^*) \mathbf{v}_{k\ell} \mathbf{v}_{k\ell}^H \text{diag}(\mathbf{x}) \mathbf{Q}_{k\ell}, \quad (40a)$$

$$\mathbf{b} = \sum_{k=1}^K \sum_{\ell=1}^L w_{k\ell} D_{k\ell} e^{i\psi_{k\ell}} \mathbf{Q}_{k\ell}^H \text{diag}(\mathbf{x}^*) \mathbf{v}_{k\ell}, \quad (40b)$$

the sub-problem to be solved here can be equivalently written in the following compact form

$$\begin{aligned} \min_{\mathbf{s} \in \mathbb{C}^{JN}} & \{\mathbf{s}^H \mathbf{A} \mathbf{s} - 2\Re(\mathbf{s}^H \mathbf{b})\}, \\ \text{s.t. } & \|\mathbf{s}\|^2 \leq NP. \end{aligned} \quad (41)$$

We have a convex quadratic function (since $\mathbf{A} \succeq 0$) that is to be minimized over a ball, and this convex problem can readily be solved as follows. Let $\mathbf{U} \mathbf{\Sigma} \mathbf{U}^H$ be the eigenvalue decomposition of \mathbf{A} , where $\mathbf{U} \in \mathbb{C}^{JN \times JN}$ is unitary, and $\mathbf{\Sigma} = \text{diag}(\sigma_1 \cdots \sigma_{JN})$, with $\sigma_i \geq 0$, for all i , and let $\tilde{\mathbf{s}} = \mathbf{U}^H \mathbf{s}$ and $\tilde{\mathbf{b}} = \mathbf{U}^H \mathbf{b}$. Then, it is not difficult to show that $\mathbf{s} = \mathbf{U} \tilde{\mathbf{s}}$ is a solution to Problem (41) if $\tilde{\mathbf{s}}$ is chosen as follows.

- If

$$\sum_{\substack{i=1 \\ \sigma_i \neq 0}}^{JN} \frac{|\tilde{b}_i|^2}{\sigma_i^2} > NP, \quad \text{or } \tilde{b}_i \neq 0$$

$$\text{for some } i \text{ such that } \sigma_i = 0, \quad (42)$$

then $\tilde{s}_i = \tilde{b}_i / (\sigma_i + \lambda)$, for all i , where $\lambda > 0$ is the unique solution of

$$\sum_{i=1}^{JN} \frac{|\tilde{b}_i|^2}{(\sigma_i + \lambda)^2} = NP. \quad (43)$$

- Otherwise, if (42) does not hold, $\tilde{s}_i = \tilde{b}_i/\sigma_i$ for all i such that $\sigma_i \neq 0$, and $\tilde{s}_i = 0$, for all i such that $\sigma_i = 0$.

The proof is reported in Appendix B.

Notice that the computational complexity for evaluating \mathbf{A} and \mathbf{b} in (40) is $\mathcal{O}(KL(MJN + J^2N^2))$, while the cost for solving Problem (41) is dominated by the eigenvalue decomposition and is equal to $\mathcal{O}(J^3N^3)$, whereby the overall computational complexity is $\mathcal{O}(KL(MJN + J^2N^2) + J^3N^3)$. Also, notice that, if (42) holds, upper and lower bounds to the optimal Lagrange multiplier λ obtained from the equation in (43) are available (see also [65]). Indeed, since

$$NP = \sum_{i=1}^{JN} \frac{|\tilde{b}_i|^2}{(\sigma_i + \lambda)^2} \leq \sum_{i=1}^{JN} \frac{|\tilde{b}_i|^2}{(\sigma_{\min} + \lambda)^2} = \frac{\|\mathbf{b}\|^2}{(\sigma_{\min} + \lambda)^2}, \quad (44)$$

where $\sigma_{\min} = \min_{i=1, \dots, JN} \sigma_i$, we have that

$$\lambda \leq \frac{\|\mathbf{b}\|}{\sqrt{NP}} - \sigma_{\min}. \quad (45)$$

Similarly, since

$$NP = \sum_{i=1}^{JN} \frac{|\tilde{b}_i|^2}{(\sigma_i + \lambda)^2} \geq \frac{1}{(\sigma_{\min} + \lambda)^2} \sum_{\substack{i=1 \\ i:\sigma_i=\sigma_{\min}}}^{JN} |\tilde{b}_i|^2, \quad (46)$$

we have that

$$\lambda \geq \max \left\{ 0, \sqrt{\frac{1}{NP} \sum_{\substack{i=1 \\ i:\sigma_i=\sigma_{\min}}}^{JN} |\tilde{b}_i|^2} - \sigma_{\min}} \right\}. \quad (47)$$

Using these upper and lower bounds, and exploiting the fact that the left-hand side of (43) is continuous, strictly decreasing, and strictly convex for $\lambda > 0$, efficient algorithms can be devised to find the solution to (43), such as the bisection method.

B. Minimization over the RIS phases

Since $\text{diag}(\mathbf{x})\mathbf{Q}_{k\ell}\mathbf{s} = \text{diag}(\mathbf{Q}_{k\ell}\mathbf{s})\mathbf{x}$, the sub-problem to be solved here is

$$\min_{\mathbf{x} \in \mathbb{C}^M} \sum_{k=1}^K \sum_{\ell=1}^L w_{k\ell} |D_{k\ell} e^{i\psi_{k\ell}} - \mathbf{v}_{k\ell}^H \text{diag}(\mathbf{Q}_{k\ell}\mathbf{s})\mathbf{x}|^2, \quad (48)$$

s.t. $|x_i| = 1, \quad i = 1, \dots, M.$

Upon defining $\mathbf{c}_{k\ell} = \text{diag}(\mathbf{Q}_{k\ell}\mathbf{s})^* \mathbf{v}_{k\ell}$, and

$$\mathbf{B} = \sum_{k=1}^K \sum_{\ell=1}^L w_{k\ell} \begin{bmatrix} \mathbf{c}_{k\ell} \mathbf{c}_{k\ell}^H & -D_{k\ell} e^{i\psi_{k\ell}} \mathbf{c}_{k\ell} \\ -D_{k\ell} e^{-i\psi_{k\ell}} \mathbf{c}_{k\ell}^H & D_{k\ell}^2 \end{bmatrix}, \quad (49)$$

Problem (48) can also be re-written in a compact form as

$$\min_{\mathbf{x} \in \mathbb{C}^M} [\mathbf{x}^H \mathbf{1}] \mathbf{B} [\mathbf{x}^T \mathbf{1}]^T, \quad (50)$$

s.t. $|x_i| = 1, \quad i = 1, \dots, M,$

that is equivalent to

$$\min_{\mathbf{x} \in \mathbb{C}^M, \xi \in \mathbb{R}} [e^{-i\xi} \mathbf{x}^H \quad e^{-i\xi}] \mathbf{B} [e^{i\xi} \mathbf{x}^T \quad e^{i\xi}]^T, \quad (51)$$

s.t. $|x_i| = 1, \quad i = 1, \dots, M,$

Algorithm 2 Coordinate descent for Problem (50)

```

choose  $\mathbf{z} \in \mathbb{C}^{M+1} : |z_i| = 1, \forall i$ 
repeat
  for  $i = 1, \dots, M+1$  do
     $z_i = \mathcal{P}_T \left( -\sum_{j=1, j \neq i}^{M+1} B_{ij} z_j \right)$ 
  end for
until convergence
set  $\mathbf{x} \in \mathbb{C}^M$  as  $x_i = z_i/|z_i|, \forall i$ 
return  $\mathbf{x}$ 

```

i.e., to

$$\min_{\mathbf{z} \in \mathbb{C}^{M+1}} \mathbf{z}^H \mathbf{B} \mathbf{z}, \quad (52)$$

s.t. $|z_i| = 1, \quad i = 1, \dots, M+1.$

If \mathbf{z}^* solves (52), the solution to Problem (50) can be recovered as $x_i^* = z_i^*/z_{M+1}^*, i = 1, \dots, M.$

Problem (52) is a complex quadratic problem and is NP-hard in general [66], [67]. A suboptimal solution can be found using different techniques, such as projected gradient, semi-definite relaxation with randomization [67], approximation with a sequence of convex equality constrained quadratic programs [47], alternating direction method of multipliers [68], Riemmanian conjugate gradient [69], etc. Here we use the simple coordinate descent algorithm, where each entry of \mathbf{z} is iteratively minimized. Since $|z_i| = 1$, for all i ,

$$\mathbf{z}^H \mathbf{B} \mathbf{z} = B_{ii} + 2\Re \left(z_i^* \sum_{\substack{j=1 \\ j \neq i}}^{M+1} B_{ij} z_j \right) + \sum_{\substack{k=1 \\ k \neq i}}^{M+1} \sum_{\substack{j=1 \\ j \neq i}}^{M+1} z_k^* B_{kj} z_j, \quad (53)$$

and the minimization over the i -th variable is simply

$$z_i = \mathcal{P}_T \left(-\sum_{\substack{j=1 \\ j \neq i}}^{M+1} B_{ij} z_j \right). \quad (54)$$

The routine is reported in Alg. 2. This algorithm has a complexity of $\mathcal{O}(M^2)$ per iteration, with an initial cost of $\mathcal{O}(KL(MJN + M^2))$ for the evaluation of the matrix \mathbf{B} in (49), and converges to a stationary point, even if there is no guarantee that it is a global minimizer. In practice, multiple initialization points can be considered, and the *best* output is kept; also, one of the initialization points must come from the output at the previous iteration, so that the objective function in Alg. 1 is decreased at every iteration.

C. Constant-modulus illuminator signals

In Problem (36), there is an overall power constraint on the illuminators. In many cases, however, the source signals are required to be constant-modulus, and only the power allocation

among the illuminators can be optimized. In this situation, Problem (36) is recast as

$$\begin{aligned}
& \min_{\mathbf{s} \in \mathbb{C}^{JN}, \mathbf{x} \in \mathbb{C}^{MN}} \sum_{k=1}^K \sum_{\ell=1}^L w_{k\ell} (D_{k\ell} - |\mathbf{v}_{k\ell}^H \text{diag}(\mathbf{x}) \mathbf{Q}_{k\ell} \mathbf{s}|)^2, \\
& \text{s.t. } |s_j| = |s_{j+J}| = \dots = |s_{j+(N-1)J}|, \\
& \hspace{15em} \text{for } j = 1, \dots, J, \\
& \|\mathbf{s}\|^2 \leq NP, \\
& |x_i| = 1, \quad i = 1, \dots, M.
\end{aligned} \tag{55}$$

This problem can sub-optimally be solved by introducing the auxiliary variables $\{\psi_{k\ell}\}_{k,\ell}$ and then using Alg. 1, where the optimization of the variable \mathbf{s} in Sec. III-A can be tackled as follows.

Let $\mathbf{u} \in \mathbb{R}^J$ be the amplitude vector of the illuminator signals, and let $\boldsymbol{\omega} \in \mathbb{C}^{JN}$ be the unit-modulus complex scalars accounting for the phase terms; then, we have

$$\mathbf{s} = \text{diag}(\boldsymbol{\omega}(\mathbf{1}_N \otimes \mathbf{I}_J))\mathbf{u} = (\mathbf{I}_N \otimes \text{diag}(\mathbf{u}))\boldsymbol{\omega}, \tag{56}$$

and the minimization problem over the variable \mathbf{s} becomes

$$\begin{aligned}
& \min_{\substack{\mathbf{u} \in \mathbb{R}^J, \boldsymbol{\omega} \in \mathbb{C}^{JN}, \\ \mathbf{s} \in \mathbb{C}^{JN}}} \{ \mathbf{s}^H \mathbf{A} \mathbf{s} - 2\Re(\mathbf{s}^H \mathbf{b}) \}, \\
& \text{s.t. } \mathbf{s} = (\mathbf{I}_N \otimes \text{diag}(\mathbf{u}))\boldsymbol{\omega}, \\
& \|\mathbf{u}\|^2 \leq P, \\
& |\omega_i| = 1, \quad i = 1, \dots, M,
\end{aligned} \tag{57}$$

where \mathbf{A} and \mathbf{b} are defined in (40). This problem can be sub-optimally solved in different ways. E.g., we can use a projected gradient algorithm: the routine is reported in Alg. 3, where η is the step size, which can be selected with a backtracking Armijo line search, and

$$\nabla_1 = 2\Re((\mathbf{1}_N^T \otimes \mathbf{I}_J) \text{diag}(\boldsymbol{\omega}^*)(\mathbf{A}\mathbf{s} - \mathbf{b})) \tag{58a}$$

$$\nabla_2 = 2(\mathbf{I}_N \otimes \text{diag}(\mathbf{u}))(\mathbf{A}\mathbf{s} - \mathbf{b}) \tag{58b}$$

are the partial derivatives of the objective function of Problem (57) with respect to \mathbf{u} and $\boldsymbol{\omega}$, respectively, with \mathbf{s} defined as in (56).

The computational complexity of Alg. 3 is dominated by the matrix-vector multiplication $\mathbf{A}\mathbf{s}$, that is needed to evaluate the the partial derivatives in (58) and the objective function; the cost per iteration is, therefore, $\mathcal{O}(J^2N^2)$.

IV. PERFORMANCE ANALYSIS

In this section, we present a numerical example to demonstrate the advantages of the RIS-based transmit architecture in Fig. 1 compared to possible competitors. In particular, the simulation setup is described in the next section; in Sec. IV-B, the benchmark systems are introduced, along with the corresponding beampattern optimization problems; finally, in Sec. IV-C, the simulation results are presented and discussed.

Algorithm 3 Projected gradient for Problem (57)

```

choose  $\mathbf{u} \in \mathbb{R}^J : \|\mathbf{u}\|^2 \leq P$ 
choose  $\boldsymbol{\omega} \in \mathbb{C}^{JN} : |\omega_i| = 1, \forall i$ 
 $\mathbf{s} = (\mathbf{I}_N \otimes \text{diag}(\mathbf{u}))\boldsymbol{\omega}$ 
repeat
  select  $\eta$ 
   $\nabla_1 = 2\Re((\mathbf{1}_N^T \otimes \mathbf{I}_J) \text{diag}(\boldsymbol{\omega}^*)(\mathbf{A}\mathbf{s} - \mathbf{b}))$ 
   $\nabla_2 = 2(\mathbf{I}_N \otimes \text{diag}(\mathbf{u}))(\mathbf{A}\mathbf{s} - \mathbf{b})$ 
   $\mathbf{u} = \mathcal{P}_{B, \sqrt{P}}(\mathbf{u} - \eta \nabla_1)$ 
   $\boldsymbol{\omega} = \mathcal{P}_T(\boldsymbol{\omega} - \eta \nabla_2)$ 
   $\mathbf{s} = (\mathbf{I}_N \otimes \text{diag}(\mathbf{u}))\boldsymbol{\omega}$ 
until convergence
return  $\mathbf{s}$ 

```

A. System settings

We consider here a 10×10 transmitting RIS, so that $M = 100$, illuminated by $J = 4$ sources. The signals have duration $T = 0.64 \mu\text{s}$ and bandwidth $W = 100$ MHz, so that $N = \lceil WT \rceil = 64$. The carrier frequency is $f_c = 3$ GHz, and the inter-element spacing of the RIS is half-wavelength of the highest frequency, i.e., $c/(2(f_c + W/2)) \approx 4.915$ cm. The 4 sources are placed at a distance of 60 cm from the RIS, each in correspondence with one of the four quadrants of the RIS. All the elements of the RIS and of the illuminator have a cosine power beampattern, and

$$\begin{aligned}
G_{ij}(f) = & \underbrace{\frac{e^{-2\pi i f d_{ij}/c}}{\sqrt{4\pi d_{ij}^2}}}_{(a)} \left(\underbrace{2(\beta + 1) \cos^\beta \theta_{j \rightarrow i} \cos^\beta \varphi_{j \rightarrow i}}_{(b)} \right. \\
& \left. \times \underbrace{\left(\frac{(c/f)^2}{4\pi} 4 \cos \theta_{i \rightarrow j} \cos \varphi_{i \rightarrow j} \right)^{1/2}}_{(c)} \right), \tag{59}
\end{aligned}$$

$$\Gamma_i(\theta, \varphi) = (4 \cos \theta \cos \varphi)^{1/2}, \tag{60}$$

where: (a) accounts for the free-space propagation, with d_{ij} the distance between the i -th element of the RIS and the j -th source; (b) is the gain of the j -th source towards the i -th element of the RIS, with $\beta = 13$, and $\theta_{j \rightarrow i}$ and $\varphi_{j \rightarrow i}$ the elevation and azimuth angles of element i of the RIS as seen from element j of the illuminator, respectively; and (c) is the effective aperture of the i -th element of the RIS from the direction of the j -th source, with $\theta_{i \rightarrow j}$ and $\varphi_{i \rightarrow j}$ the elevation and azimuth angles of element j of the illuminator as seen from element i of the RIS, respectively. Notice that the elements of the source and of the RIS are in each other far-field, but not the whole source and RIS, whereby the channel $G_{ij}(f)$ describes a spherical-wave propagation.

The desired beampattern is composed of a broad beam for the negative frequencies and a narrow beam for all frequencies;

more precisely,

$$D(f; \theta, \varphi) = \begin{cases} \frac{16}{\sqrt{W(\sqrt{2-\sin \frac{\pi}{8}})}}, & \text{if } (f, \theta, \varphi) \in [-\frac{W}{2}, 0] \\ & \times [0, \frac{\pi}{4}] \times [-\frac{\pi}{4}, 0] \\ & \text{or if } (f, \theta, \varphi) \in [-\frac{W}{2}, \frac{W}{2}] \\ & \times [-\frac{\pi}{4}, \frac{\pi}{8}] \times [\frac{\pi}{8}, \frac{\pi}{4}] \\ 0, & \text{otherwise.} \end{cases} \quad (61)$$

The power radiated with the desired beampattern is, therefore,

$$\frac{1}{4\pi} \int_{-W/2}^{W/2} \int_{-\pi/2}^{\pi/2} \int_{-\pi/2}^{\pi/2} d^2(f; \theta, \varphi) \cos \theta d\theta d\varphi df = 8W. \quad (62)$$

The available power is $P = 10W$, and the weighting function is $\tilde{w}(f; \theta, \varphi) = 1$, so that, from (62), Eq. (33) becomes $w(f; \theta, \varphi) = (W\pi \cos \theta)/(32KL)$. The number of frequency sampling points is $K = 128$, and they are uniformly spaced in¹⁰ $[-W/2, W/2]$; in the angular domain, 36×36 sampling points uniformly spaced in $[-\pi/2, \pi/2]^2$ are taken,¹¹ so that $L = 1296$.

In all figures, we plot the normalized power beampattern (NPB), i.e., the power beampattern normalized by its maximum value

$$\text{NPB}(f; \theta, \varphi) = \frac{B^2(f; \theta, \varphi)}{\max_{\{f', \theta', \varphi'\}} B^2(f'; \theta', \varphi')}. \quad (63)$$

Finally, the convergence criterion adopted for Alg. 1 is to stop when either the objective function or all the dependent variables experience a relative change between consecutive iterations smaller than 10^{-6} .

B. Benchmark

For the sake of comparison, we also consider the cases of a MIMO system and of a phased array (PA), both having M elements with position \mathbf{p}_i and power beampattern $4 \cos \theta \cos \varphi$, $i = 1, \dots, M$. Let $\zeta_i(t)$ be the waveform sent over the i -th element of the array, and define

$$\zeta_n = [\zeta_1(n/W) \cdots \zeta_M(n/W)]^T \in \mathbb{C}^M, \quad (64a)$$

$$\zeta = [\zeta_1^T \cdots \zeta_M^T]^T \in \mathbb{C}^{MN}, \quad (64b)$$

$$\tilde{\mathbf{Q}}(f; \theta, \varphi) = \frac{\sqrt{4 \cos \theta \cos \varphi}}{W\sqrt{T}} (\mathbf{e}^T(f) \otimes \mathbf{I}_M) \in \mathbb{C}^{M \times MN}. \quad (64c)$$

Then, it is not difficult to show that the amplitude beampattern of the MIMO system and of the PA can be expressed in both cases as $|\mathbf{v}^H(f; \theta, \varphi) \tilde{\mathbf{Q}}(f; \theta, \varphi) \zeta|$. Such a beampattern is optimized according to the same criterion used for the

¹⁰Observe that 128 is roughly twice the number of sampling points needed to uniformly sample the source signals at the Nyquist rate.

¹¹Notice that the smallest half-power beamwidth of a uniformly excited, equally spaced linear array with 10 elements and half-wavelength spacing is approximately equal to $0.891 \frac{2}{10} \approx 0.1782$ rad [63, Eq. (2.100)]; therefore, 36 is roughly twice the number of sampling points needed to uniformly sample the interval $[-\pi/2, \pi/2]$ with a 0.1782 rad spacing.

illuminator and RIS architecture considered in Sec. II. In particular, the optimization problem for the MIMO system is

$$\begin{aligned} \min_{\zeta \in \mathbb{C}^{MN}} \quad & \sum_{k=1}^K \sum_{\ell=1}^L w_{k\ell} (D_{k\ell} - |\mathbf{v}_{k\ell}^H \tilde{\mathbf{Q}}_{k\ell} \zeta|)^2, \\ \text{s.t.} \quad & \|\zeta\|^2 \leq NP, \end{aligned} \quad (65)$$

where $\tilde{\mathbf{Q}}_{k\ell} = \tilde{\mathbf{Q}}(f_k; \theta_\ell, \varphi_\ell)$, and, if constant-modulus waveforms are required,

$$\begin{aligned} \min_{\zeta \in \mathbb{C}^{MN}} \quad & \sum_{k=1}^K \sum_{\ell=1}^L w_{k\ell} (D_{k\ell} - |\mathbf{v}_{k\ell}^H \tilde{\mathbf{Q}}_{k\ell} \zeta|)^2, \\ \text{s.t.} \quad & |\zeta_i| = |\zeta_{i+M}| = \cdots = |\zeta_{i+(N-1)M}|, \\ & \text{for } i = 1, \dots, M, \\ & \|\zeta\|^2 \leq NP. \end{aligned} \quad (66)$$

These problems are solved here as in Sec. III: specifically, the auxiliary variables $\{\psi_{k\ell}\}_{k,\ell}$ are first introduced, and then a block-coordinate descent method is adopted, where the minimization over ζ is carried out as in Sec. III-A and III-C for Problem (65) and (66), respectively.¹²

In PAs, the space-time signal ζ is bounded to have a special structure, i.e., $\zeta = \boldsymbol{\rho} \otimes \boldsymbol{\chi}$, where $\boldsymbol{\rho} \in \mathbb{C}^N$ represents the transmit waveform, and $\boldsymbol{\chi} \in \mathbb{C}^M$, with $|\chi_i| = 1$ for all i , is the beamforming vector. The optimization problem for the PA is

$$\begin{aligned} \min_{\substack{\boldsymbol{\rho} \in \mathbb{C}^N, \boldsymbol{\chi} \in \mathbb{C}^M \\ \zeta \in \mathbb{C}^{MN}}} \quad & \sum_{k=1}^K \sum_{\ell=1}^L w_{k\ell} (D_{k\ell} - |\mathbf{v}_{k\ell}^H \tilde{\mathbf{Q}}_{k\ell} \zeta|)^2, \\ \text{s.t.} \quad & \zeta = \boldsymbol{\rho} \otimes \boldsymbol{\chi}, \\ & |\chi_i| = 1, \quad i = 1, \dots, M, \\ & \|\boldsymbol{\rho}\|^2 \leq NP/M, \end{aligned} \quad (67)$$

and, if constant-modulus waveforms are required,

$$\begin{aligned} \min_{\substack{\boldsymbol{\rho} \in \mathbb{C}^N, \boldsymbol{\chi} \in \mathbb{C}^M \\ \alpha \in \mathbb{R}, \zeta \in \mathbb{C}^{MN}}} \quad & \sum_{k=1}^K \sum_{\ell=1}^L w_{k\ell} (D_{k\ell} - |\mathbf{v}_{k\ell}^H \tilde{\mathbf{Q}}_{k\ell} \zeta|)^2, \\ \text{s.t.} \quad & \zeta = \alpha \boldsymbol{\rho} \otimes \boldsymbol{\chi}, \\ & |\chi_i| = 1, \quad i = 1, \dots, M, \\ & |\rho_i| = 1, \quad i = 1, \dots, N, \\ & \alpha^2 \leq P/M. \end{aligned} \quad (68)$$

These problems are again solved by introducing the auxiliary variables $\{\psi_{k\ell}\}_{k,\ell}$ and then using a block-coordinate descent method. Specifically, for Problem (67), the minimizations over $\boldsymbol{\rho}$ and $\boldsymbol{\chi}$ are carried out as in Sec. III-A and III-B, respectively. For Problem (68), instead, the minimizations over $\boldsymbol{\rho}$ and $\boldsymbol{\chi}$ are

¹²The computational complexity required for Problem (65) is $\mathcal{O}(KLM^2N)$ for updating $\{\psi_{k\ell}\}_{k,\ell}$ and $\mathcal{O}(KLM^2N^2 + M^3N^3)$ for updating ζ . For Problem (66), instead, the ζ -update with the projected gradient method requires a complexity of $\mathcal{O}(M^2N^2)$ per iteration plus an initial cost of $\mathcal{O}(KLM^2N^2)$.

tackled as in Sec. III-B, while the minimization over α simply gives¹³

$$\alpha = \min \left\{ \sqrt{\frac{P}{M}}, \frac{\sum_{k=1}^K \sum_{\ell=1}^L w_{k\ell} D_{k\ell} \Re(e^{-i\psi_{k\ell}} \mathbf{v}_{k\ell}^H \tilde{\mathbf{Q}}_{k\ell} (\mathbf{e} \otimes \boldsymbol{\chi}))}{\sum_{k=1}^K \sum_{\ell=1}^L w_{k\ell} |\mathbf{v}_{k\ell}^H \tilde{\mathbf{Q}}_{k\ell} (\mathbf{e} \otimes \boldsymbol{\chi})|^2} \right\}. \quad (69)$$

C. Numerical results

The following figures have been drawn using 128 frequency grid points uniformly spaced in $[-W/2, W/2]$ and 144×144 grid points uniformly spaced in $[-\pi, \pi]^2$. Fig. 2 shows a 3-D plot of the NPB as a function of the azimuth and elevation for two frequency cuts: the wide beam (for the negative frequencies) and the narrow beam (for all frequencies) are clearly visible and well-shaped, and the sidelobes are relatively low.

The next figures, instead, report 2-D intensity plots of the desired NPB (first row) and of the NPB synthesized with the RIS-based transmit architecture (second row) and with the considered benchmarks, i.e., MIMO system (third row) and PA (fourth row). Specifically, Figs. 3, 4, and 5 show the NPB as a function of the azimuth and elevation for two frequencies (-25 MHz in the left column, 25 MHz in the right column), as a function of the frequency and azimuth for two elevations (-33.75° in the left column, 22.5° in the right column), and as a function of the frequency and elevation for two azimuths (-22.5° in the left column, 33.75° in the right column). Clearly, thanks to the higher number of degrees of freedom, the MIMO system is able to realize the beampattern most similar to the desired one, with well-shaped beams, sharp transitions between the two frequency regions, and low sidelobes. The worst performance is obtained with the PA, due to the limited number of degrees of freedom for the beampattern design problem, and this is particularly evident in the frequency domain.¹⁴ The results achieved with the RIS-based architecture lie in between these two cases, as can also be seen from the RSE reported in Table I (second column).¹⁵

Finally, Figs. 6, 7, and 8 replicate Figs. 3, 4, and 5 for the case where constant-modulus illuminator signals are used. Clearly, due to the additional constraint, the realized

¹³The computational complexity for Problem (67) requires an initial cost of $\mathcal{O}(KLM^2N)$; then the cost is $\mathcal{O}(KLM^2N)$ for updating $\{\psi_{k\ell}\}_{k,\ell}$, $\mathcal{O}(M^2N + N^2)$ for updating \mathbf{e} , and, if the coordinate descent method is used, $\mathcal{O}(M^2)$ per iteration for updating $\boldsymbol{\chi}$ plus an initial cost of $\mathcal{O}(M^2)$. For Problem (68), instead, the \mathbf{e} -update with the coordinate descent method requires a complexity of $\mathcal{O}(N^2)$ per iteration plus an initial cost of $\mathcal{O}(M^2N + N^2 + KL)$, and there is an additional update for α , that requires a cost of $\mathcal{O}(KLMN)$.

¹⁴Here, we are only concerned with the mathematical model, and PA is just a particular case of MIMO, so its performance is necessarily worse due to the reduced number of degrees of freedom. However, PAs are not outdated (especially in radar applications) due to their simplicity and reliability in challenging environments.

¹⁵The power radiated by the sources (not reported in the table) to obtain the desired beampattern is approximately equal to the available power for all considered systems. Notice, however, that the radiated power is, in general, a small fraction of the overall power budget needed to operate the arrays, and fully digital MIMO systems are known to be much more demanding in terms of overall power requirement than RIS-based transmitters [15].

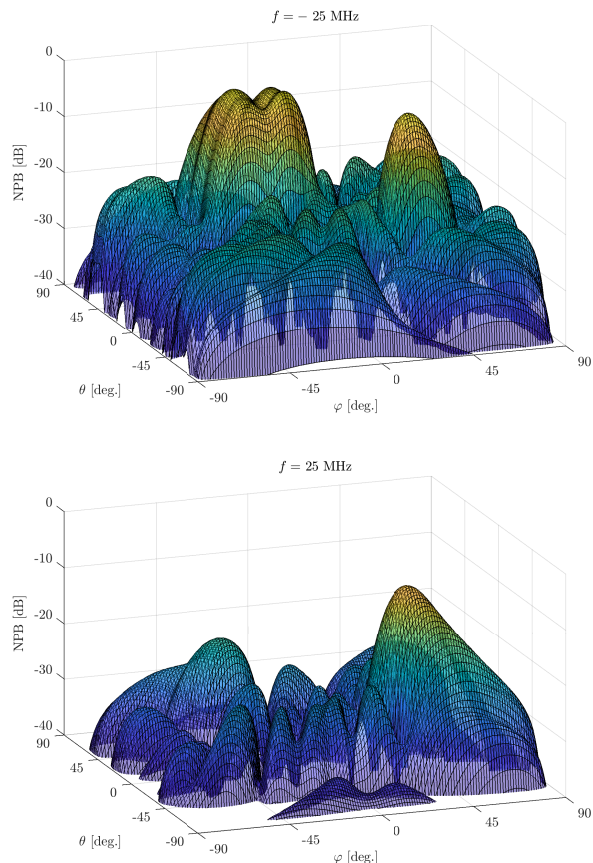


Figure 2. Normalized power beampattern (synthesized with the RIS-based architecture) as a function of elevation and azimuth at frequencies -25 MHz (top) and 25 MHz (bottom).

Table I
RELATIVE SQUARE ERROR

System	RSE	RSE with constant-modulus signals
RIS-based	Problem (36): 0.21	Problem (55): 0.25
MIMO	Problem (65): 0.14	Problem (66): 0.23
PA	Problem (67): 0.27	Problem (68): 0.35

beampattern is worse for all three systems, with a higher ripple in the frequency domain. Specifically, the MIMO system exhibits the largest relative loss compared to the corresponding non-constant-modulus case, as can also be seen from Table I. The RIS-based architecture, which already has an *intrinsic* constant-modulus constraint on the RIS phases, better bears the reduction in the available degrees of freedom caused by the additional constraint. In particular, the beampattern realized with the RIS-based architecture using only 4 active sources looks similar to the one realized with the MIMO system that exploits 100 active sources, as it can also be seen from the RSE, that is much closer to the MIMO system than to PA.

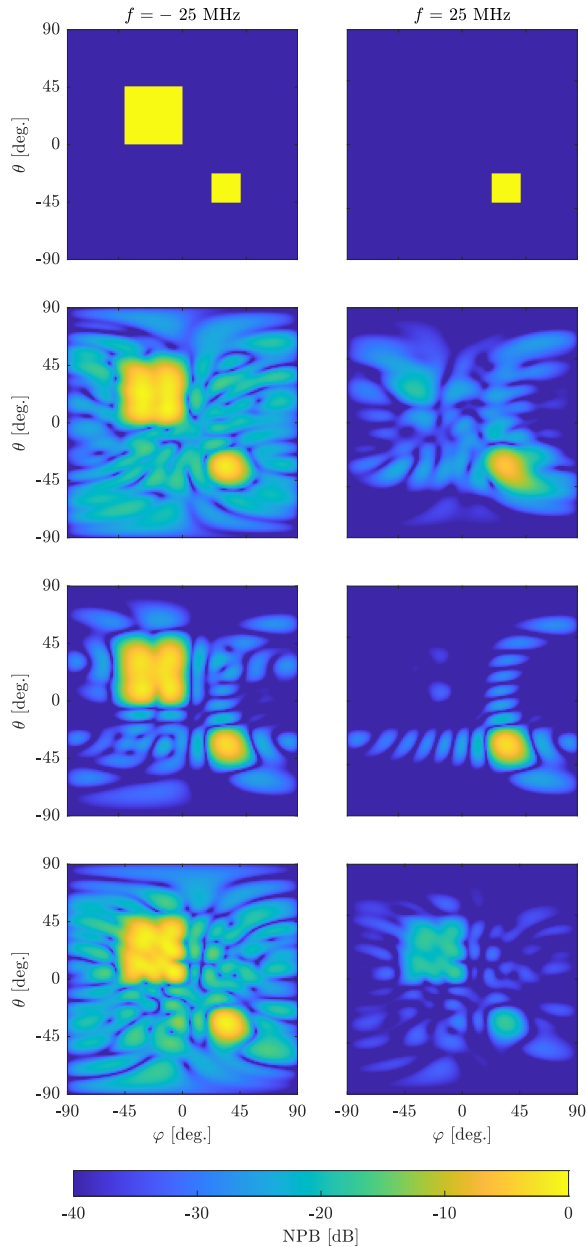


Figure 3. Desired (top row) and synthesized with the RIS-based architecture (second row), with a MIMO system (third row), and with a phased array (bottom row) normalized power beampattern as a function of elevation and azimuth at frequencies -25 MHz (left column) and 25 MHz (right column).

V. CONCLUSION

In this work, we have tackled the problem of beampattern design in a system where a large reflecting/transmitting RIS is illuminated by a small number of active sources. It has been shown that satisfactory performance in terms of relative square error between the desired and the realized beampattern can be achieved with this RIS-based transmit architecture. Furthermore, the presented example with 4 sources and a 100-element RIS has shown that the realized beampattern is not dramatically different from the beampattern realized

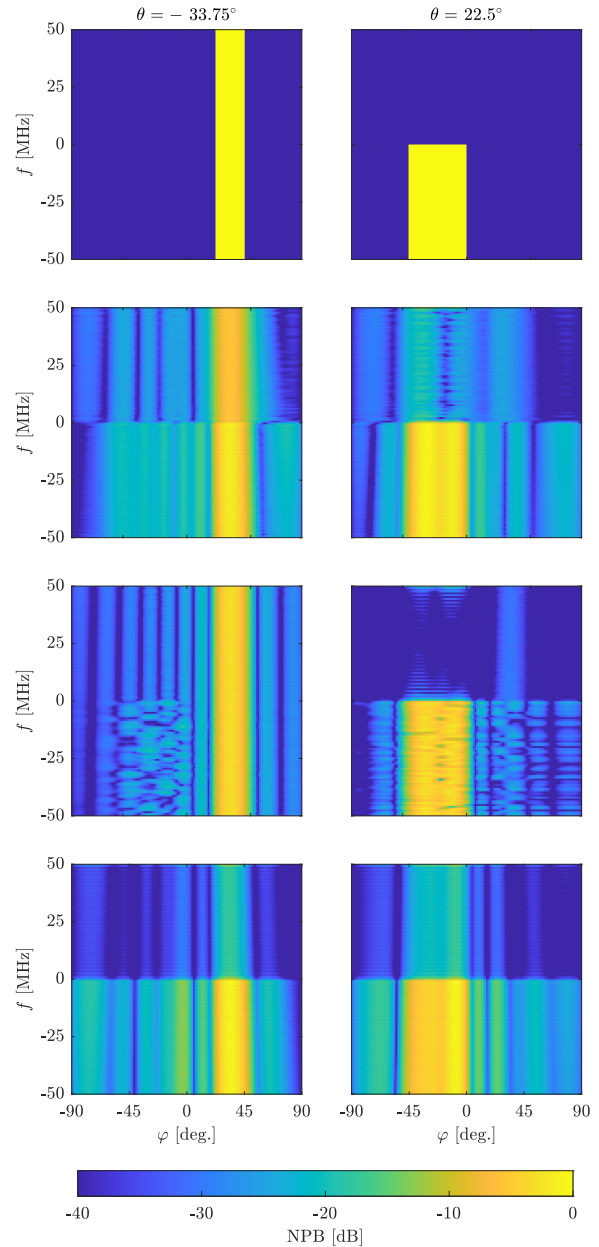


Figure 4. Desired (top row) and synthesized with the RIS-based architecture (second row), with a MIMO system (third row), and with a phased array (bottom row) normalized power beampattern as a function of frequency and azimuth at elevations -33.75° (left column) and 22.5° (right column).

with an equivalent MIMO system with 100 active elements. This architecture is, therefore, very promising in reducing the costs when elaborated beampatterns need to be synthesized. Future works will focus on optimizing the position and number of source signals and on adopting active RISs, which grant additional degrees of freedom and are known to deliver better performance when the distances between the sources and the RIS are large.

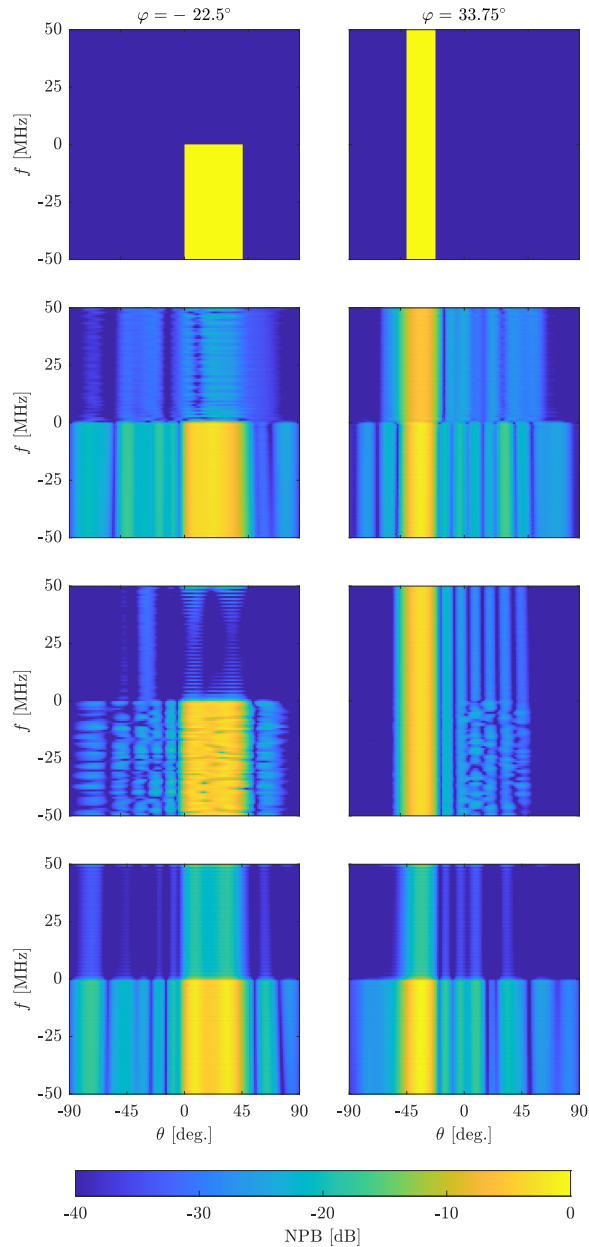


Figure 5. Desired (top row) and synthesized with the RIS-based architecture (second row), with a MIMO system (third row), and with a phased array (bottom row) normalized power beampattern as a function of frequency and elevation at azimuths -22.5° (left column) and 33.75° (right column).

APPENDIX A

ALTERNATIVE SUB-OPTIMUM SOLUTION TO PROBLEM (38)

In the block-coordinate descent method, multiple choices of the block-coordinate variables are possible if a solution (at least sub-optimum) to the corresponding sub-problems is available. In our case, an alternative choice (with respect to the one made in Sec. III) for Problem (38) can be represented by the auxiliary variables $\{\psi_{k\ell}\}$ and the pair $\{\mathbf{s}, \mathbf{x}\}$. Indeed, the minimization over $\{\psi_{k\ell}\}$ is again solved by (39). As for the minimization over $\{\mathbf{s}, \mathbf{x}\}$, instead, we can resort to the

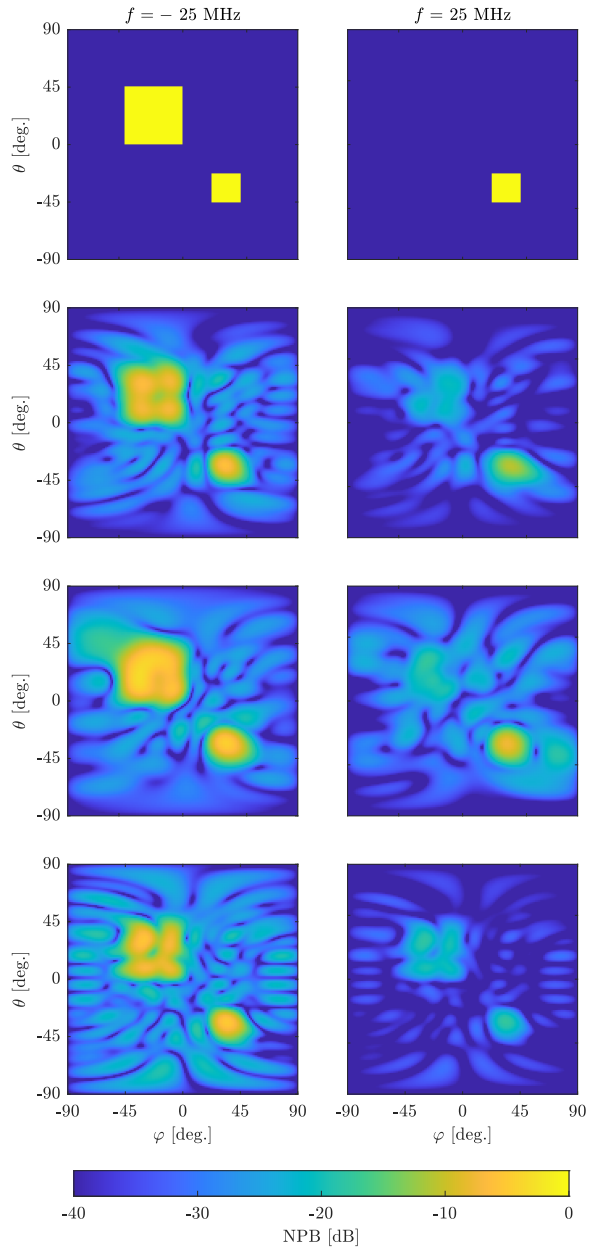


Figure 6. Desired (top row) and synthesized with the RIS-based architecture (second row), with a MIMO system (third row), and with a phased array (bottom row) normalized power beampattern as a function of elevation and azimuth at frequencies -25 MHz (left column) and 25 MHz (right column) when constant-modulus illuminator signals are used.

projected gradient method to obtain a sub-optimum solution. The complete routine (block-coordinate descent in the outer loop and projected gradient in the inner loop) is reported in Alg. 4, where

$$\begin{aligned} \nabla_1 = 2 \sum_{k=1}^K \sum_{\ell=1}^L w_{k\ell} (\mathbf{v}_{k\ell}^H \text{diag}(\mathbf{x}) \mathbf{Q}_{k\ell} \mathbf{s} - D_{k\ell} e^{i\psi_{k\ell}})^2 \\ \times \mathbf{Q}_{k\ell}^H \text{diag}(\mathbf{x}^*) \mathbf{v}_{k\ell} \end{aligned} \quad (70a)$$

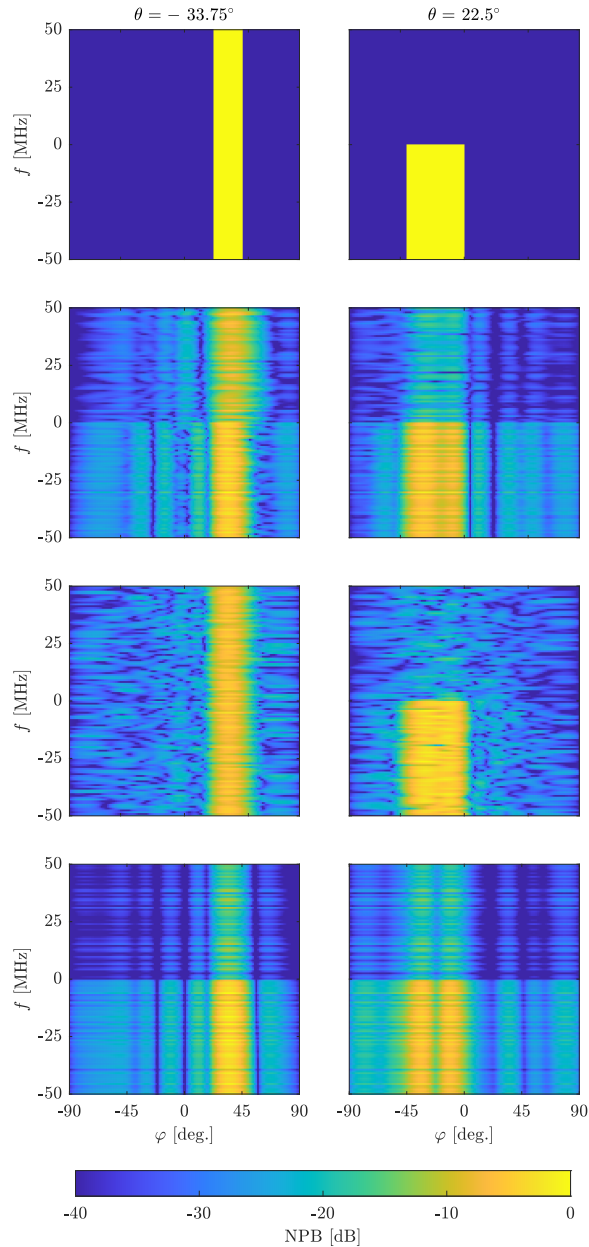


Figure 7. Desired (top row) and synthesized with the RIS-based architecture (second row), with a MIMO system (third row), and with a phased array (bottom row) normalized power beampattern as a function of frequency and azimuth at elevations -33.75° (left column) and 33.75° (right column) when constant-modulus illuminator signals are used.

$$\nabla_2 = 2 \sum_{k=1}^K \sum_{\ell=1}^L w_{k\ell} (\mathbf{v}_{k\ell}^H \text{diag}(\mathbf{x}) \mathbf{Q}_{k\ell} \mathbf{s} - D_{k\ell} e^{i\psi_{k\ell}})^2 \times \text{diag}(\mathbf{Q}_{k\ell} \mathbf{s})^* \mathbf{v}_{k\ell} \quad (70b)$$

are the partial derivatives of the objective function of Problem (38) with respect to \mathbf{s} and \mathbf{x} , respectively.

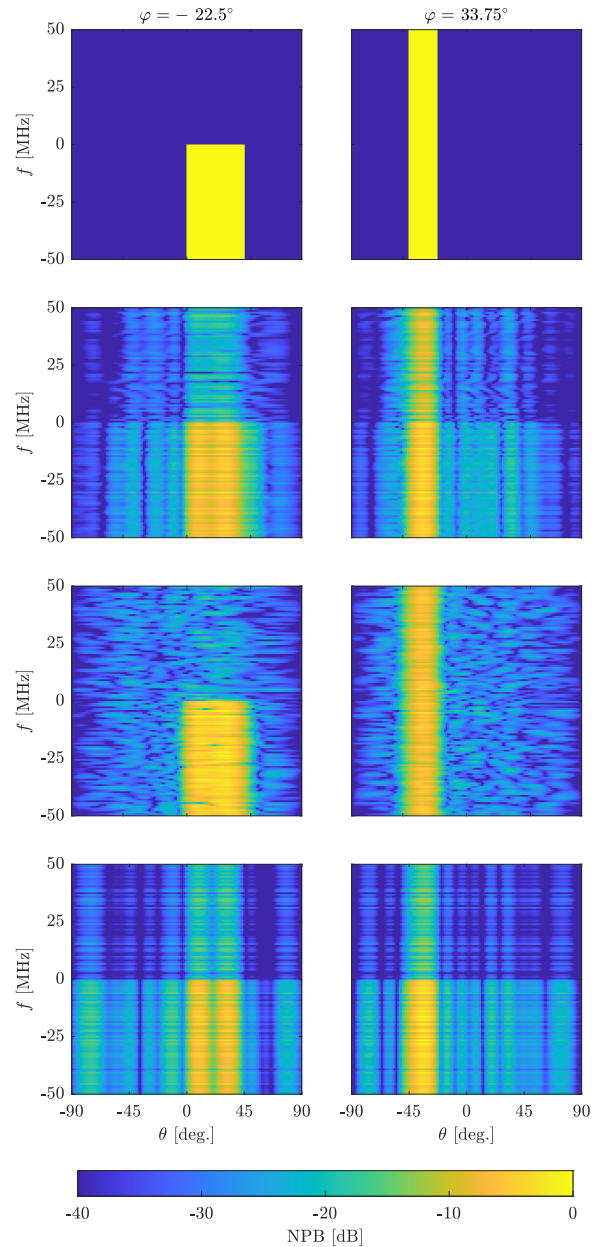


Figure 8. Desired (top row) and synthesized with the RIS-based architecture (second row), with a MIMO system (third row), and with a phased array (bottom row) normalized power beampattern as a function of frequency and elevation at azimuths -33.75° (left column) and 33.75° (right column) when constant-modulus illuminator signals are used.

APPENDIX B SOLUTION TO PROBLEM (41)

Recalling that $\tilde{\mathbf{s}} = \mathbf{U}^H \mathbf{s}$ and $\tilde{\mathbf{b}} = \mathbf{U}^H \mathbf{b}$, Problem (41) can be recast as

$$\begin{aligned} \min_{\tilde{\mathbf{s}} \in \mathbb{C}^{JN}} & \sum_{i=1}^{JN} \left(\sigma_i |\tilde{s}_i|^2 - 2\Re(\tilde{b}_i \tilde{s}_i^*) \right), \\ \text{s.t.} & \sum_{i=1}^{JN} |\tilde{s}_i|^2 \leq NP, \end{aligned} \quad (71)$$

Algorithm 4 Block-coordinate descent for Problem (38)

choose $\mathbf{s} \in \mathbb{C}^{JN} : \|\mathbf{s}\|^2 \leq NP$
 choose $\mathbf{x} \in \mathbb{C}^M : |x_i| = 1 \forall i$
 $\psi_{k\ell} = \arg(\mathbf{v}_{k\ell}^H \text{diag}(\mathbf{x}) \mathbf{Q}_{k\ell} \mathbf{s}), \forall k, \ell$
repeat
repeat
 select η
 $\nabla_1 = 2 \sum_{k=1}^K \sum_{\ell=1}^L w_{k\ell} (\mathbf{v}_{k\ell}^H \text{diag}(\mathbf{x}) \mathbf{Q}_{k\ell} \mathbf{s} - D_{k\ell} e^{i\psi_{k\ell}})^2 \mathbf{Q}_{k\ell}^H \text{diag}(\mathbf{x}^*) \mathbf{v}_{k\ell}$
 $\nabla_2 = 2 \sum_{k=1}^K \sum_{\ell=1}^L w_{k\ell} (\mathbf{v}_{k\ell}^H \text{diag}(\mathbf{x}) \mathbf{Q}_{k\ell} \mathbf{s} - D_{k\ell} e^{i\psi_{k\ell}})^2 \text{diag}(\mathbf{Q}_{k\ell} \mathbf{s})^* \mathbf{v}_{k\ell}$
 $\mathbf{s} = \mathcal{P}_{B, \sqrt{P}}(\mathbf{s} - \eta \nabla_1)$
 $\mathbf{x} = \mathcal{P}_T(\mathbf{x} - \eta \nabla_2)$
 $\psi_{k\ell} = \arg(\mathbf{v}_{k\ell}^H \text{diag}(\mathbf{x}) \mathbf{Q}_{k\ell} \mathbf{s}), \forall k, \ell$
until convergence
until convergence
return \mathbf{s} and \mathbf{x}

and the Karun-Kush-Tucker conditions are

$$\begin{cases} (\sigma_i + \lambda) \tilde{s}_i = \tilde{b}_i, & i = 1, \dots, JN, \\ \lambda \geq 0, \\ \sum_{i=1}^{JN} |\tilde{s}_i|^2 \leq NP, \\ \lambda \left(\sum_{i=1}^{JN} |\tilde{s}_i|^2 - NP \right) = 0. \end{cases} \quad (72)$$

At this point, upon introducing the function

$$f(\lambda) = \sum_{i=1}^{JN} \frac{|\tilde{b}_i|^2}{(\sigma_i + \lambda)^2}, \quad (73)$$

we can distinguish between the following cases.

- 1) If $\sigma_i > 0$ for all i and $f(0) \leq NP$, we can take $\lambda = 0$ and then $\tilde{s}_i = \tilde{b}_i / \sigma_i$;
- 2) If $\sigma_i > 0$ for all i and $f(0) > NP$, then $\lambda > 0$, and it must be chosen so that $f(\lambda) = NP$, while $\tilde{s}_i = \tilde{b}_i / (\sigma_i + \lambda)$, for any i ; notice that, since f is strictly decreasing, and $f(0) > NP$, the equation $f(\lambda) = NP$ admits a unique solution.
- 3) If $\sigma_i = 0$ for some i , and there exists i such that $\sigma_i = 0$ and $\tilde{b}_i \neq 0$, then $\lambda > 0$, and it must be chosen so that $f(0) = NP$, while $\tilde{s}_i = \tilde{b}_i / (\sigma_i + \lambda)$; since f is strictly decreasing, and $\lim_{\lambda \rightarrow 0} f(\lambda) = \infty$, the equation $f(\lambda) = NP$ admits a unique solution.
- 4) If $\sigma_i = 0$ for some i , $\tilde{b}_i = 0$ for all i such that $\sigma_i = 0$, and $\sum_{i=1, i: \sigma_i > 0}^{JN} |\tilde{b}_i|^2 / \sigma_i^2 \leq NP$, we can take $\lambda = 0$ and then $\tilde{s}_i = \tilde{b}_i / \sigma_i$, if $\sigma_i > 0$, while it can be arbitrarily set equal to zero, if $\sigma_i = 0$.
- 5) If $\sigma_i = 0$ for some i , $\tilde{b}_i = 0$ for all i such that $\sigma_i = 0$, and $\sum_{i=1, i: \sigma_i > 0}^{JN} |\tilde{b}_i|^2 / \sigma_i^2 > NP$, then $\lambda > 0$, and it must be chosen so that $f(0) = NP$, while $\tilde{s}_i = \tilde{b}_i / (\sigma_i + \lambda)$; since f is strictly decreasing, and $\lim_{\lambda \rightarrow 0} f(\lambda) = \infty$, the equation $f(\lambda) = NP$ admits a unique solution.

Finally, these five cases can be condensed as follows: if (42) holds, then $\tilde{s}_i = \tilde{b}_i / (\sigma_i + \lambda)$, for all i , where $\lambda > 0$ is the unique solution of $f(\lambda) = NP$, while, if (42) does not hold, $\tilde{s}_i = \tilde{b}_i / \sigma_i$ for all i such that $\sigma_i \neq 0$, and $\tilde{s}_i = 0$, for all i such that $\sigma_i = 0$.

REFERENCES

- [1] S. Blackman and R. Popoli, *Design and analysis of modern tracking systems*. Artech House, 1999.
- [2] M. Shafi *et al.*, "5G: A tutorial overview of standards, trials, challenges, deployment, and practice," *IEEE J. Sel. Topics Signal Process.*, vol. 35, no. 6, pp. 1201–1221, 2017.
- [3] W. Saad, M. Bennis, and M. Chen, "A vision of 6G wireless systems: Applications, trends, technologies, and open research problems," *IEEE Netw.*, vol. 34, no. 3, pp. 134–142, 2020.
- [4] C. Chaccour *et al.*, "Seven defining features of terahertz (THz) wireless systems: A fellowship of communication and sensing," *IEEE Commun. Surveys Tuts.*, vol. 24, no. 2, pp. 967–993, 2022.
- [5] S. Jin and S. Roy, "FMCW radar network: Multiple access and interference mitigation," *IEEE J. Sel. Topics Signal Process.*, vol. 15, no. 4, pp. 968–979, 2021.
- [6] H. Wei, N. Deng, and M. Haenggi, "Performance analysis of inter-cell interference coordination in mm-Wave cellular networks," *IEEE Trans. Wireless Commun.*, vol. 21, no. 2, pp. 726–738, 2022.
- [7] E. Grossi, M. Lops, and L. Venturino, "Energy efficiency optimization in radar-communication spectrum sharing," *IEEE Trans. Signal Process.*, vol. 69, pp. 3541–3554, 2021.
- [8] A. Hassanien, M. Amin, Y. Zhang, and F. Ahmad, "Dual-function radar-communications: Information embedding using sidelobe control and waveform diversity," *IEEE Trans. Signal Process.*, vol. 64, no. 8, pp. 2168–2181, 2016.
- [9] J. Johnston, L. Venturino, E. Grossi, M. Lops, and X. Wang, "MIMO OFDM dual-function radar-communication under error rate and beam-pattern constraints," *IEEE J. Sel. Topics Signal Process.*, vol. 40, no. 6, pp. 1951–1964, 2022.
- [10] F. Liu *et al.*, "Integrated sensing and communications: Toward dual-functional wireless networks for 6G and beyond," *IEEE J. Sel. Topics Signal Process.*, vol. 40, no. 6, pp. 1728–1767, 2022.
- [11] X. Gao, L. Dai, and A. M. Sayeed, "Low RF-complexity technologies to enable millimeter-wave MIMO with large antenna array for 5G wireless communications," *IEEE Commun. Mag.*, vol. 56, no. 4, pp. 211–217, 2018.
- [12] O. E. Ayach, S. Rajagopal, S. Abu-Surra, Z. Pi, and R. W. Heath, "Spatially sparse precoding in millimeter wave MIMO systems," *IEEE Trans. Wireless Commun.*, vol. 13, no. 3, pp. 1499–1513, 2014.
- [13] A. F. Molisch *et al.*, "Hybrid beamforming for massive MIMO: A survey," *IEEE Commun. Mag.*, vol. 55, no. 9, pp. 134–141, 2017.
- [14] H. Yan, S. Ramesh, T. Gallagher, C. Ling, and D. Cabric, "Performance, power, and area design trade-offs in millimeter-wave transmitter beamforming architectures," *IEEE Circuits Syst. Mag.*, vol. 19, no. 2, pp. 33–58, 2019.
- [15] V. Jamali, A. M. Tulino, G. Fischer, R. R. Müller, and R. Schober, "Intelligent surface-aided transmitter architectures for millimeter-wave ultra massive MIMO systems," *IEEE Open J. Commun. Soc.*, vol. 2, pp. 144–167, 2021.
- [16] M. Di Renzo *et al.*, "Smart radio environments empowered by reconfigurable intelligent surfaces: How it works, state of research, and the road ahead," *IEEE J. Sel. Areas Commun.*, vol. 38, no. 11, pp. 2450–2525, 2020.
- [17] E. Basar and H. V. Poor, "Present and future of reconfigurable intelligent surface-empowered communications [perspectives]," *IEEE Signal Process. Mag.*, vol. 38, no. 6, pp. 146–152, 2021.
- [18] J. Huang and J. A. Encinar, *Reflectarray antennas*. Hoboken, NJ, USA: John Wiley & Sons, Inc., 2007.
- [19] S. V. Hum and J. Perruisseau-Carrier, "Reconfigurable reflectarrays and array lenses for dynamic antenna beam control: A review," *IEEE Trans. Antennas Propag.*, vol. 62, no. 1, pp. 183–198, 2014.
- [20] P. Nayeri, F. Yang, and A. Z. Elsherbeni, "Beam-scanning reflectarray antennas: A technical overview and state of the art," *IEEE Trans. Antennas Propag.*, vol. 57, no. 4, pp. 32–47, 2015.
- [21] Q. He, S. Sun, and L. Zhou, "Tunable/reconfigurable metasurfaces: Physics and applications," *Research*, vol. 2019, 2019.
- [22] O. Tsilipakos *et al.*, "Toward intelligent metasurfaces: The progress from globally tunable metasurfaces to software-defined metasurfaces with an embedded network of controllers," *Adv. Opt. Mater.*, vol. 8, no. 17, p. 2000783, 2020.
- [23] R. Long, Y.-C. Liang, Y. Pei, and E. G. Larsson, "Active reconfigurable intelligent surface-aided wireless communications," *IEEE Trans. Wireless Commun.*, vol. 20, no. 8, pp. 4962–4975, 2021.
- [24] K. Liu, Z. Zhang, L. Dai, S. Xu, and F. Yang, "Active reconfigurable intelligent surface: Fully-connected or sub-connected?" *IEEE Commun. Lett.*, vol. 26, no. 1, pp. 167–171, 2022.

- [25] Z. Zhang *et al.*, “Active RIS vs. passive RIS: Which will prevail in 6G?” *IEEE Trans. Commun.*, vol. 71, no. 3, pp. 1707–1725, 2023.
- [26] T. J. Cui, M. Q. Qi, X. Wan, J. Zhao, and Q. Cheng, “Coding metamaterials, digital metamaterials and programmable metamaterials,” *Light: Sci. & Appl.*, vol. 3, no. 10, p. e218, 2014.
- [27] X. Xie *et al.*, “Joint precoding for active intelligent transmitting surface empowered outdoor-to-indoor communication in mmwave cellular networks,” *IEEE Trans. Wireless Commun.*, vol. 22, no. 10, pp. 7072–7086, 2023.
- [28] S. Abeywickrama, R. Zhang, Q. Wu, and C. Yuen, “Intelligent reflecting surface: Practical phase shift model and beamforming optimization,” *IEEE Trans. Wireless Commun.*, vol. 68, no. 9, pp. 5849–5863, 2020.
- [29] M. Dajer *et al.*, “Reconfigurable intelligent surface: design the channel — a new opportunity for future wireless networks,” *Digital Communications and Networks*, vol. 8, no. 2, pp. 87–104, 2022.
- [30] J. Xu, Y. Liu, X. Mu, and O. A. Dobre, “STAR-RISs: Simultaneous transmitting and reflecting reconfigurable intelligent surfaces,” *IEEE Commun. Lett.*, vol. 25, no. 9, pp. 3134–3138, 2021.
- [31] Q. Wu and R. Zhang, “Intelligent reflecting surface enhanced wireless network via joint active and passive beamforming,” *IEEE Trans. Wireless Commun.*, vol. 18, no. 11, pp. 5394–5409, 2019.
- [32] Y. Liu *et al.*, “Reconfigurable intelligent surfaces: Principles and opportunities,” *IEEE Commun. Surveys Tuts.*, vol. 23, no. 3, pp. 1546–1577, 2021.
- [33] X. Ma, S. Guo, H. Zhang, Y. Fang, and D. Yuan, “Joint beamforming and reflecting design in reconfigurable intelligent surface-aided multi-user communication systems,” *IEEE Trans. Wireless Commun.*, vol. 20, no. 5, pp. 3269–3283, 2021.
- [34] R. Schroeder, J. He, G. Brante, and M. Juntti, “Two-stage channel estimation for hybrid RIS assisted MIMO systems,” *IEEE Trans. Commun.*, vol. 70, no. 7, pp. 4793–4806, 2022.
- [35] X. Guo, Y. Chen, and Y. Wang, “Wireless beacon enabled hybrid sparse channel estimation for RIS-aided mmwave communications,” *IEEE Trans. Commun.*, vol. 71, no. 5, pp. 3144–3160, 2023.
- [36] A. H. Abdelrahman, F. Yang, A. Z. Elsherbeni, and P. Nayeri, *Analysis and Design of Transmitarray Antennas*, ser. Synthetic Lectures on Antennas. Morgan & Claypool Publishers, 2017.
- [37] K. T. Pham *et al.*, “Low-cost metal-only transmitarray antennas at K-band,” *IEEE Antennas Wireless Propag. Lett.*, vol. 18, no. 6, pp. 1243–1247, 2019.
- [38] H. Hasani, J. S. Silva, S. Capdevila, M. García-Vigueras, and J. R. Mosig, “Dual-band circularly polarized transmitarray antenna for satellite communications at (20, 30) GHz,” *IEEE Trans. Antennas Propag.*, vol. 67, no. 8, pp. 5325–5333, 2019.
- [39] Q. Li, M. Wen, and M. Di Renzo, “Single-RF MIMO: From spatial modulation to metasurface-based modulation,” *IEEE Trans. Wireless Commun.*, vol. 28, no. 4, pp. 88–95, 2021.
- [40] P. Stoica, J. Li, and Y. Xie, “On probing signal design for MIMO radar,” *IEEE Trans. Signal Process.*, vol. 55, no. 8, pp. 4151–4161, 2007.
- [41] D. R. Fuhrmann and G. San Antonio, “Transmit beamforming for MIMO radar systems using signal cross-correlation,” *IEEE Trans. Aerosp. Electron. Syst.*, vol. 44, no. 1, pp. 171–186, 2008.
- [42] S. Ahmed and M.-S. Alouini, “MIMO radar transmit beampattern design without synthesizing the covariance matrix,” *IEEE Trans. Signal Process.*, vol. 62, no. 9, pp. 2278–2289, 2014.
- [43] A. Aubry, A. De Maio, and Y. Huang, “MIMO radar beampattern design via PSL/ISL optimization,” *IEEE Trans. Signal Process.*, vol. 64, no. 15, pp. 3955–3967, 2016.
- [44] Z. Cheng, Z. He, S. Zhang, and J. Li, “Constant modulus waveform design for MIMO radar transmit beampattern,” *IEEE Trans. Signal Process.*, vol. 65, no. 18, pp. 4912–4923, 2017.
- [45] G. San Antonio and D. Fuhrmann, “Beampattern synthesis for wideband MIMO radar systems,” in *IEEE Int. Workshop Comput. Adv. Multi-Sensor Adapt. Process. (CAMSAP)*, 2005, pp. 105–108.
- [46] H. He, P. Stoica, and J. Li, “Wideband MIMO systems: Signal design for transmit beampattern synthesis,” *IEEE Trans. Signal Process.*, vol. 59, no. 2, pp. 618–628, Feb. 2011.
- [47] O. Aldayel, V. Monga, and M. Rangaswamy, “Tractable transmit MIMO beampattern design under a constant modulus constraint,” *IEEE Trans. Signal Process.*, vol. 65, no. 10, pp. 2588–2599, 2017.
- [48] K. Alhujaili, V. Monga, and M. Rangaswamy, “Transmit MIMO radar beampattern design via optimization on the complex circle manifold,” *IEEE Trans. Signal Process.*, vol. 67, no. 13, pp. 3561–3575, 2019.
- [49] B. Guo and J. Li, “Waveform diversity based ultrasound system for hyperthermia treatment of breast cancer,” *IEEE Trans. Biomed. Eng.*, vol. 55, no. 2, pp. 822–826, 2008.
- [50] X. Liu *et al.*, “Joint transmit beamforming for multiuser MIMO communications and MIMO radar,” *IEEE Trans. Signal Process.*, vol. 68, 2020.
- [51] X. Wang, Z. Fei, Z. Zheng, and J. Guo, “Joint waveform design and passive beamforming for RIS-assisted dual-functional radar-communication system,” *IEEE Trans. Veh. Technol.*, vol. 70, no. 5, pp. 5131–5136, 2021.
- [52] G. Zhang, C. Shen, F. Liu, Y. Lin, and Z. Zhong, “Beampattern design for RIS-aided dual-functional radar and communication systems,” in *IEEE Global Commun. Conf. (GLOBECOM)*, 2022, pp. 3899–3904.
- [53] H. Luo, R. Liu, M. Li, Y. Liu, and Q. Liu, “Joint beamforming design for RIS-assisted integrated sensing and communication systems,” *IEEE Trans. Veh. Technol.*, vol. 71, no. 12, pp. 13 393–13 397, 2022.
- [54] M. Rahal *et al.*, “Arbitrary beam pattern approximation via RISs with measured element responses,” in *Joint Europ. Conf. Netw. Commun. & 6G Summit (EuCNC/6G Summit)*, 2022.
- [55] E. Grossi and L. Venturino, “Beampattern design for radars with reconfigurable intelligent surfaces,” in *IEEE Radar Conf. (RadarConf)*, 2023.
- [56] S. Buzzi, E. Grossi, M. Lops, and L. Venturino, “Radar target detection aided by reconfigurable intelligent surfaces,” *IEEE Signal Process. Lett.*, vol. 28, pp. 1315–1319, 2021.
- [57] A. Aubry, A. De Maio, and M. Rosamilia, “Reconfigurable intelligent surfaces for N-LOS radar surveillance,” *IEEE Trans. Veh. Technol.*, vol. 70, no. 10, pp. 10 735–10 749, 2021.
- [58] S. Buzzi, E. Grossi, M. Lops, and L. Venturino, “Foundations of MIMO radar detection aided by reconfigurable intelligent surfaces,” *IEEE Trans. Signal Process.*, vol. 70, pp. 1749–1763, 2022.
- [59] M. Rihan, E. Grossi, L. Venturino, and S. Buzzi, “Spatial diversity in radar detection via active reconfigurable intelligent surfaces,” *IEEE Signal Process. Lett.*, vol. 29, pp. 1242–1246, 2022.
- [60] S. Gao, X. Cheng, and L. Yang, “Spatial multiplexing with limited RF chains: Generalized beamspace modulation (GBM) for mmWave massive MIMO,” *IEEE J. Sel. Areas Commun.*, vol. 37, no. 9, pp. 2029–2039, 2019.
- [61] J. Wang, L. He, and J. Song, “Towards higher spectral efficiency: Spatial path index modulation improves Millimeter-Wave hybrid beamforming,” *IEEE J. Sel. Topics Signal Process.*, vol. 13, no. 6, pp. 1348–1359, 2019.
- [62] R. Liu, M. Li, H. Luo, Q. Liu, and A. L. Swindlehurst, “Integrated sensing and communication with reconfigurable intelligent surfaces: Opportunities, applications, and future directions,” *IEEE Wireless Commun.*, vol. 30, no. 1, pp. 50–57, 2023.
- [63] H. L. V. Trees, *Optimum array processing: Part IV of Detection, Estimation, and Modulation Theory*. New York, NY, USA: John Wiley & Sons, Inc., 2002.
- [64] D. P. Bertsekas, *Nonlinear Programming*, 2nd ed. Belmont, MA, USA: Athena Scientific, 1999.
- [65] W. W. Hager, “Minimizing a quadratic over a sphere,” *SIAM J. Optim.*, vol. 12, no. 1, pp. 188–208, 2001.
- [66] S. Zhang and Y. Huang, “Complex quadratic optimization and semidefinite programming,” *SIAM J. Optimization*, vol. 16, no. 3, pp. 871–890, 2006.
- [67] Z.-Q. Luo and T.-H. Chang, “SDP relaxation of homogeneous quadratic optimization: approximation bounds and applications,” in *Convex Optimization in Signal Processing and Communications*, D. P. Palomar and Y. C. Eldar, Eds. Cambridge, UK: Cambridge University Press, 2010, ch. 4, pp. 117–165.
- [68] J. Liang, H. C. So, J. Li, and A. Farina, “Unimodular sequence design based on alternating direction method of multipliers,” *IEEE Trans. Signal Process.*, vol. 64, no. 20, pp. 5367–5381, 2016.
- [69] J. Wu, S. Kim, and B. Shim, “Energy-efficient power control and beamforming for reconfigurable intelligent surface-aided uplink IoT networks,” *IEEE Trans. Wireless Commun.*, vol. 21, no. 12, pp. 10 162–10 176, 2022.